Assessing and managing risks with transitions in flood defence infrastructure

Quantifying the probability of failure at asset transitions

Reliability analysis (performance assessment) of flood defence transitions

Date: March 2023

Version: FRS17181/R3

We are the Environment Agency. We protect and improve the environment.

We help people and wildlife adapt to climate change and reduce its impacts, including flooding, drought, sea level rise and coastal erosion.

We improve the quality of our water, land and air by tackling pollution. We work with businesses to help them comply with environmental regulations. A healthy and diverse environment enhances people's lives and contributes to economic growth.

We can't do this alone. We work as part of the Defra group (Department for Environment, Food & Rural Affairs), with the rest of government, local councils, businesses, civil society groups and local communities to create a better place for people and wildlife.

Author(s):
Jonathan Simm, Mohamed Hassan

Research at the Environment Agency

Scientific research and analysis underpins everything the Environment Agency does. It helps us to understand and manage the environment effectively. Our own experts work with leading scientific organisations, universities and other parts of the Defra group to bring the best knowledge to bear on the environmental problems that we face now and in the future. Our scientific work is published as summaries and reports, freely available to all.

This report is the result of research commissioned and funded by the Joint Flood and Coastal Erosion Risk Management Research and Development Programme. The Joint Programme is jointly overseen by Defra, the Environment Agency, Natural Resources Wales and Welsh Government on behalf of all risk management authorities in England and Wales: Flood and Coastal Erosion Risk Management Research and Development Programme

You can find out more about our current science programmes at https://www.gov.uk/government/organisations/environment-agency/about/research

If you have any comments or questions about this report or the Environment Agency's other scientific work, please contact research@environment-agency.gov.uk.

Dr Robert Bradburne
Chief Scientist

Foreword

This report signposts potentially relevant considerations for practitioners when managing portfolios of flood risk assets with transitions. It is not intended to be, and should not be read as, prescriptive, exhaustive, or a statement of best practice.

The research findings presented in this report were commissioned by the Environment Agency for this project. This document is one of four outputs from this project and must be read alongside those other research outputs, rather than considered in isolation.

The outputs from this project are being used by the Environment Agency to review and improve our internal management processes. We apply a risk-based approach to all our activities, ensuring public money is targeted in a way to achieve the most benefit. This means that we may conclude that some of the techniques set out in this document are not appropriate for the Environment Agency to use.

Contents

Figures

Tables

1. Introduction

Project overview

Transitions between flood defence assets and components introduce irregularities which increase the chance of failure, as seen in many historic flood events. Current guidance in England and Wales on the visual inspection of flood defence assets to determine condition does not explicitly account for the potential effects of transitions on defence performance. As such, where transitions do increase the probability of defence failure above that of the adjoining defence assets, the associated risks are missed from local, regional, and national flood risk assessments. This research supports identifying, prioritising and assessing flood defence asset transitions to determine if they form a weak spot compared to the neighbouring assets and therefore could lead to increased flood risk. Quantifying the increased failure risk due to the transitions then feeds into a next step of prioritisation for improvement works.

The aims of the project are to:

- consider the presence of transitions when assessing flood defence condition
- quantify the effects of transitions on defence performance (fragility) and flood risk
- manage the risk of transitions with improved design and retrofitted solutions for existing defences

The research outputs have been divided into 4 reports. Each report focuses on a different stage of managing assets at transitions (Figure 1-1). This report focuses on quantification of transition failure probability for use in screening and inspection and post inspection and prioritisation, and outlines the reliability of the inspection process.
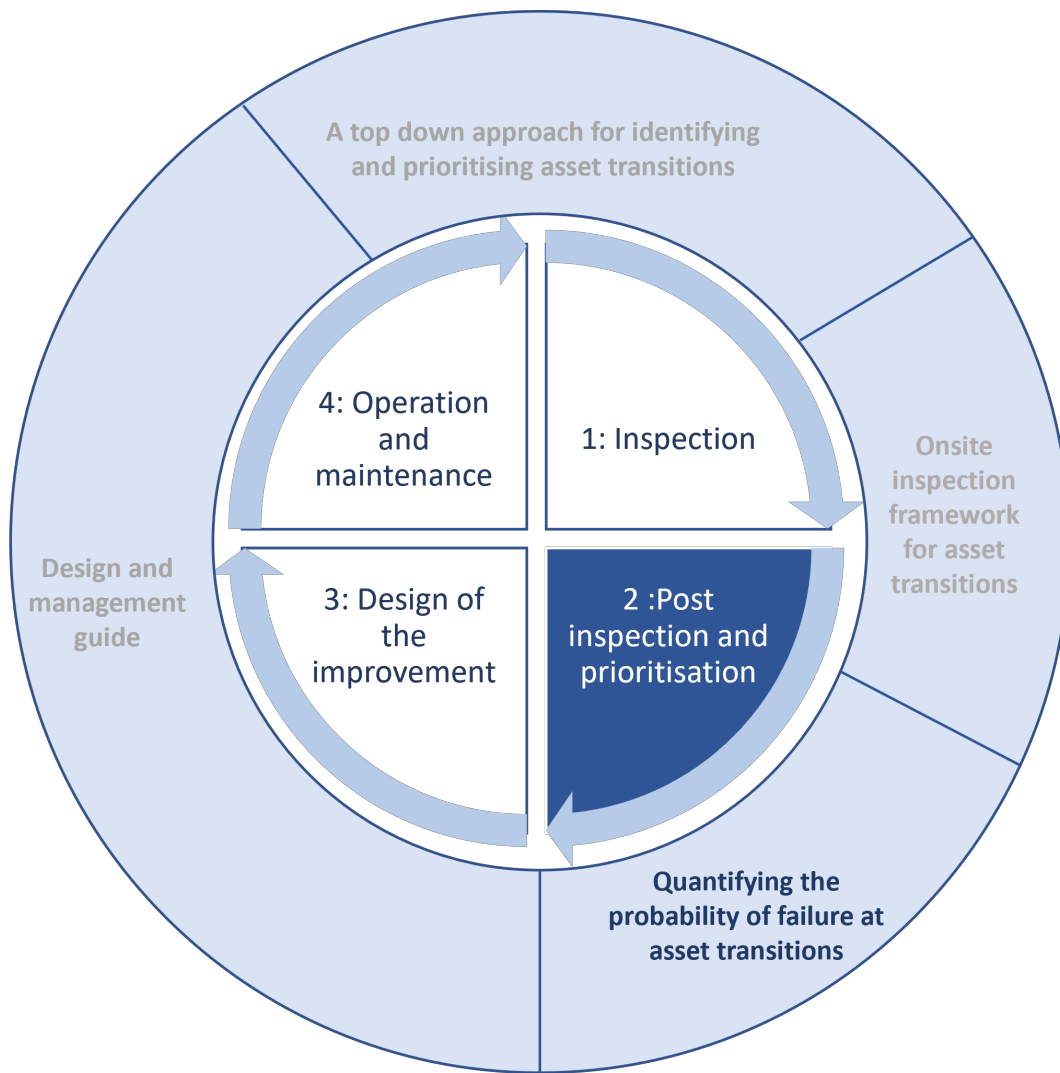
Figure Error! Use the Home tab to apply 0 to the text that you want to appear here.**.1 project overview**

Scope of report

Although it is widely acknowledged that embankment failures are more likely to occur at points of change (transitions), there has been relatively little monitoring, physical testing or numerical or physical modelling of these assets and their failure modes with which equations representing their reliability can be constructed.

This report documents the research carried out to develop the science of fragility curves for transitions, focusing on the influences on loading conditions and impacts on resistance to damage. The research process documented in this report has involved:

- reviewing relevant literature
- consulting with international experts at project workshops
- learning from computational fluid dynamic (CFD) modelling of a typical channel to assess the hydrodynamic performance of the overflow at the transition between a levee

(grass embankment) and a flood wall (vertical wall). The main objectives of this CFD study were to assess the relative increase of flow velocities and shear stresses at these transitions, with particular interest in the grass embankment, which is the 'weaker' structure

- identifying and defining the Limit State Equations (LSEs) that represent the most important failure mechanisms for different transition types
- incorporating the modified LSEs into the hr*RELIABLE* tool to allow bespoke assessments of site-specific transition fragility curves

This report, together with the modified hr*RELIABLE* tool, the quantifying the probability of failure outputs of the transitions research project.

Who is this report for?

The envisaged users are the teams and specialists responsible for managing and programming flood defence improvements, particularly the senior engineers in any flood defence asset management organisation responsible for oversight of this work. In the specific context of the Environment Agency, this would be the catchment engineers and the Asset Performance Teams and potentially their consultants as well.

Users of this report should be familiar with the concept of fragility curves.

Using this report

As part of this project, relevant research has been reviewed to ensure that the most appropriate current science is used to inform the approach. Due to the lack of currently available research and evidence, the representation defined in this document (that has been implemented in the hr*RELIABLE* code) should be considered to be an 'initial' approach that should be reviewed and updated in the future.

Any development work by HR Wallingford on hr*RELIABLE* (intellectual property rights (IPR) owned by HR Wallingford) is being carried out with no charge to the Environment Agency.

The review in this report is focused on fluvial defence non-composite assets subject to variable but non-dynamic water level conditions (no significant waves present).

Coastal defence assets were excluded, by agreement with the Environment Agency, since at the moment coastal fragility representations are based on earlier (2004) simplified and judgement-based approaches using a univariate loading expressed in terms of overtopping rate. Multivariate fragility representations may potentially be developed in the future, but this has not been pursued under this project.

Transverse transitions occurring within the cross-section of a composite asset (for example, flood wall on top of an embankment) are also excluded from this analysis, since the performance of the composite asset has to be viewed as a whole.

The report only considers damage mechanisms that may occur during a flood event. Deterioration of assets due to a range of slow mechanisms is not directly assessed or quantified within fragility curves.

Report structure

This report is divided into 2 sections. The first section, chapters 2 to 4, provides an overview of failure mechanisms at transitions, the selection of transition types to be represented in the modelling process, and a review of relevant research. The second section, chapters 5 to 8, describes the development of the hr*RELIABLE* tool, including the parameters chosen, sensitivity analysis and results discussion.

2.   Review of failure mechanisms

This section records the considerations which have led to including some failure mechanisms (for representation by fragility curves) and excluding others.

The included failure mechanisms, which are summarised in this section and then evaluated and discussed in the remaining sections of this report, include the following:

- internal erosion in the form of concentrated leak erosion. For transitions in UK defence assets, it is believed that concentrated leak erosion will be the most common internal erosion mechanism
- external erosion of the landward face of the embankment at the transition. This does include the effect of crest degradation/lowering, leading to more severe external erosion of the landward face, although as discussed in section 3.3 this can also be viewed as a hydraulic failure (note that hydraulic failures are not represented by fragility curves)

The excluded failure mechanisms discussed in this section include:

- instability of the slope of the embankment at the transition
- instability of the hard structure at the transition
- external erosion of the water side slope

Included mechanism: concentrated leak internal erosion of the embankment at the transition

As discussed further in section 5.3, concentrated leak internal erosion is one of 4 known mechanisms for the initiation of internal erosion in flood embankments, the others being:

- under-seepage driven backward erosion (or piping)
- contact erosion
- suffusion

There is little experience internationally of flood embankments experiencing contact erosion or suffusion.

Under-seepage driven backward erosion is a well-known phenomenon with flood embankments. It arises primarily where layers of permeable sands or gravels lie beneath a relatively thin surface layer of more impermeable materials (clays and sands). These situations do arise in the UK (for example, in the Thames Estuary), but it is believed to be less common than concentrated leak erosion triggered by cracking or animal burrows. In any event, in the specific case of transitions, there is no obvious mechanism which would increase the possibility of under-seepage piping.

By contrast, concentrated leak erosion requires the existence of a pre-existing crack or low stress area which has less resistance to the applied water head when the flood embankment is loaded. Such cracks are more likely to arise at a transition than in an embankment generally due to the risk of hydraulic separation or fracture at the interface between the soil of the embankment and the adjoining hard structure. The concentrated leak erosion process involves initial erosion along the walls of the crack (ICOLD, 2016a), continuation of this erosion leading to enlargement of the crack, eventually resulting in a breach.

Included mechanism: external erosion of the landward face of the embankment at the transition

External erosion of the landward face of a flood embankment is perhaps the most obvious failure mechanism, arising when a flood embankment is overtopped and the resulting shear stress applied by the overtopping water on the rear face exceeds the capacity of the grass cover to resist it. In the USA, it is often assumed that once a flood embankment is overtopped, structural failure will occur very rapidly.

There are 3 main reasons that external erosion is likely to be worse at a transition:

■ local flow accelerations and increases in turbulence causing increased hydraulic shear stress on the landward surface

■ local crest settlement, allowing earlier overflow during flood events and associated increases in flow velocities.

■ poorer quality grass cover at the transition close to the hard structure due to light shading or difficulties with maintenance procedures

Included mechanism: crest degradation

Crest degradation is primarily a deterioration process rather than a separate failure process. The main concern with crest degradation in terms of the fragility of transitions is that, for any given water level, it allows higher velocities over the crest and rear face, leading to earlier onset of external erosion. As noted above, this process can be allowed for in the external erosion fragility curves simply by adjusting the crest elevation on the horizontal axis of the fragility curve. It is therefore not a separate 'structural' failure mechanism.

It should be noted, however, that crest degradation can also represent a 'hydraulic' failure mechanism, as it can lead to the crest level falling below that which is appropriate for the Standard of Protection of the asset. Such a hydraulic failure may mean that when flooding occurs to the Standard of Protection level (for example, the 1:100-year water level), overflow may still occur.

Excluded mechanism: slope instability

Slope instability, sometimes called 'mass instability', of the embankment part of a transition is not taken forward for further analysis for the following reasons:

- Mass instability at longitudinal transitions has almost never been reported. Failure processes at such longitudinal transitions are dominated by external and internal erosion.

- Mass instability of UK flood embankments in their own right is much rarer than external erosion or internal erosion. As described in the International Levee Handbook (ILH), the most common situations for mass instability of flood embankments to occur are (see ILH section 9.9) as follows:

  - during or immediately after construction, when pore pressures are high (due to the need to install earthworks at optimum moisture content) and may not have had time to dissipate. Such situations do not normally continue beyond the end of the construction contract defects correction period

  - during floods on the landward face of the levee due to elevated pore water pressures developing due to prolonged (weeks to months) durations of high flood levels in rivers. Such prolonged durations of exposure to elevated flood levels are extremely rare in the UK, because flood hydrographs, even in the larger rivers, rarely exceed more than a few days

  - during floods on the waterward face of the levee following external erosion of the waterward slope. As explained in section 2.3, this only occurs in situations where the embankment is close to the river bank on the outside of bend of a river. Here, the river flow can cut into the bank and eventually into the embankment itself, whereupon it can cause mass instability. However, this behaviour is localised, highly site specific and 3-dimensional

  - after floods on the waterward face of the levee, due to rapid drawdown of river water levels. While this kind of failure does occur in the UK, because it occurs after flooding, it does not have immediate consequences for flood risk. It only eventually becomes important if repair is not feasible before the next flood event comes along and even then, only if the failure removes part of the crest

  - due to seismic loading. Significant seismic loading in the UK is extremely rare and even more rare when in conjunction with a flood event, and is therefore normally disregarded in design processes

Of these processes, those progressive during or after flooding are essentially deterioration processes not included within the scope of this project. Fragility curves are only able to capture rapid processes that occur during a single, relatively short duration, flood event, whereas deterioration processes take place over a much longer period of time. Even if such deterioration processes were in scope, developing fragility curves in these cases would be a major challenge since (a) there could be a very broad range of resulting impacts on the structures and (b) it would be necessary to make

some allowance for temporary or permanent repairs probably having been carried out before a subsequent flood event.

- There is no simple way of representing mass instability in fragility curves in a generally applicable way:
  - the classical approaches (for example, Bishop's slope stability method) are implicit and very specific to the geometry and materials of the embankment
  - more advanced/complex methods (for example, finite element) are similarly specific to the geometry and materials of the embankment and require significant computational resources. Such approaches would be necessary to assess mass instability at transitions because of their highly 3-dimensional nature
- Mass instability at transverse transitions is a generally a function of the behaviour of the whole composite structure (for example, flood wall surmounting a flood embankment) and not of the transition itself. (It is noted that the one of the failure mechanisms for the I-walls in New Orleans during Hurricane Katrina was the 'pumping' of water (by the backwards and forwards motion of the wall under the impact of waves and floating objects) down the interface between the flood wall and the embankment due to the flood wall; however, the eventual failure process was of the structure as a whole).

Excluded mechanism: structure instability

This relates to instability of the hard structure part of the transition. In the case of longitudinal transitions, this will almost always not be as vulnerable to failure as the adjoining embankment or the interface between the two and therefore it is inappropriate to focus on this issue. In the case of transverse transitions (for example, embankment with surmounting flood wall), the instability of the structure is part of the instability of the composite structure as a whole and this has been agreed to be excluded from scope. If fragility curves were to be developed for instability of such structures, they would need to be based around failure mechanisms relating to one or more of the following:

- rotational mass instability of the wall and embankment combination, which could occur either quite locally to the wall or more globally
- sliding mass instability of the wall in relation to the flood embankment

Excluded mechanism: external erosion of the waterside slope

External erosion of the waterside slope is a complex mechanism, which does not lend itself readily to fragility analysis. Normally in a fluvial setting such erosion will only occur when morphological changes lead to the flow being concentrated against the levee or the river bank on which it is founded. This will arise, for example, on the outside of a river bend

and determination of the applied loading will require detailed numerical or physical modelling or careful local data collection.

Furthermore, external erosion on the water side slope tends to be a slow process, the development of which is:

a. highly specific to the exact geometrical/geotechnical arrangements at the location in question (for example, related to higher than usual velocities on the outside of a river bend or to increased turbulence due to physical protrusions into the flow associated with structures such as pipes, outfalls, abutments or related to the velocity needed to mobilise a particular sediment type)
b. identifiable (where erosion is visible above the water line) as a deterioration process during regular visual inspection (and therefore manageable during subsequent maintenance/repair activities)

3. Transition types to be represented

The transition types being used within the transitions research project are shown here in Figure 3-1:

Type 1 – Longitudinal transitions

Between embankment and flood wall   Between embankment and point asset

Type 2 – Cross-sectional transitions

Between embankment and crest wall   Between toe wall and embankment

Type 3 – Crossing infrastructure

Between embankment and crossing structure

Type 4- Revetments

Between soft and hard revetments
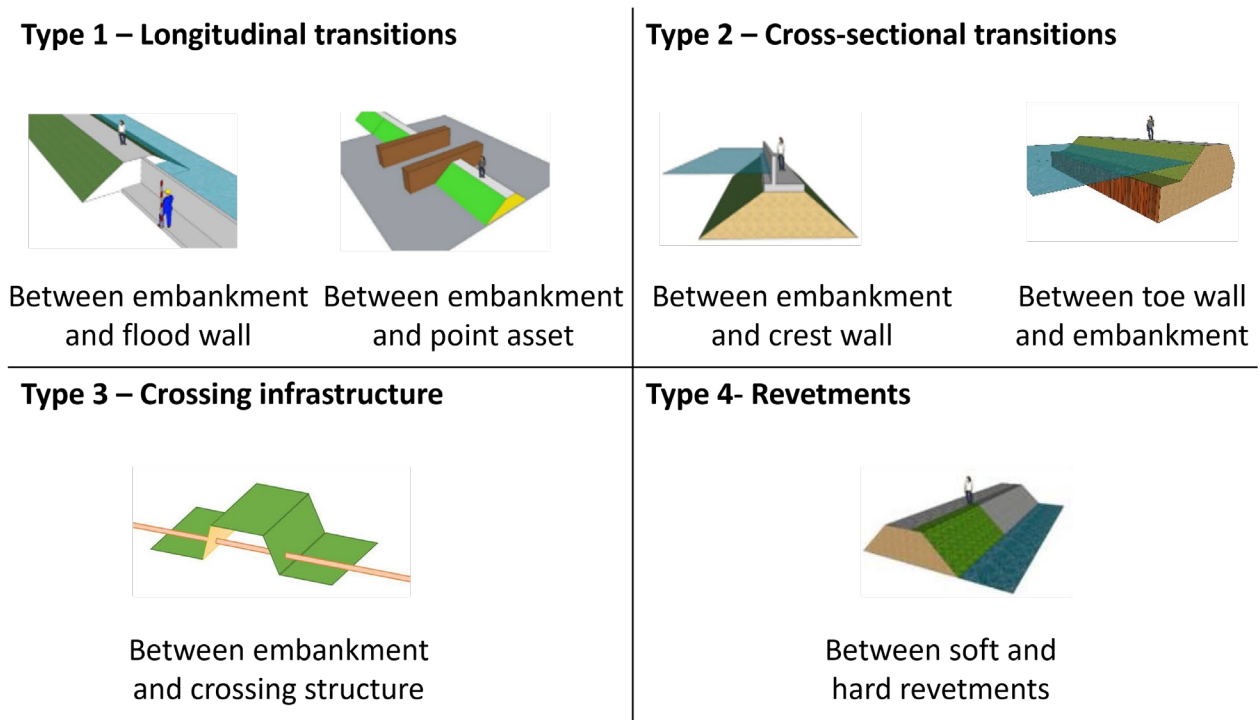
Figure Error! Use the Home tab to apply 0 to the text that you want to appear here..**2 The 4 types of transition considered in this research**

Of these 4 transition types, only the following are included within the update of the hr*RELIABLE* tool:

Transition type 1**:**   Embankment to wall or wall of point asset (where the embankment may be higher, lower or the same height as the wall).

Transition type 3**:**   An embedded object within the embankment. This could be a utility cable, pipe or culvert crossing the full width of the embankment,

Transition type 4**:**   A change in the surface covering on the external (landward) face of the embankment.

Transition type 2 relates to cross-sectional transitions which only arise in composite structures. These have been agreed to be excluded for the purposes of fragility curve generation under this project. The reason for this is that fragility curves for such composite structures need to apply to the whole structure (for example, overall instability) and due to the potential multiplicity of combinations of hard and soft elements in a composite structure, there are no common approaches. Having said this, clearly:

a. internal erosion processes are likely to be similar to those for transition type 3
b. external erosion processes are likely to be similar to those for all transition types, but with different coefficients

However, overall fragility curves for such transitions could only be generated if combined with fragility curves for such composite structures operating as a whole.

4. Relevant research

This study has drawn on the following publications:

- van Bergeijk, 2018 (The effects of transitions on wave overtopping flow and dike cover erosion for flood defence reliability - Literature report)
- Verheij and others, 2013 and van Hoven, 2015 (Evaluation and Model Development - Grass Erosion Test at the Rhine dike)
- ICOLD bulletin 164, 2015 (Internal erosion of existing dams, levees and dikes, and their foundations - Volume 1: internal erosion processes and engineering assessment)
- HR Wallingford, 2019 (Transitions in flood defences – CFD study)

It should be noted that the first 2 of these references refer to results from (unsteady) wave overtopping experiments rather than steady overflow situations relevant to fluvial situations. We discuss in detail the justification for using some outputs from this research in the rest of this section below, but the main reason for assuming transferability to the fluvial situation relates to the fact that the main coefficients relate to modifications of force or pressure rather than flow rates or velocities. We acknowledge that it is not ideal that the pressures in the unsteady situation are pulsating, whereas in the fluvial case they will be more steady. However, in the absence of other research to draw on, they are a good starting point until further testing and validation is available. We further account for factor value uncertainty by using a triangular distribution in hr*RELIABLE* (by not using a single value). The learning drawn from these documents is summarised in the following sections.

van Bergeijk, 2018 (The effects of transitions on wave overtopping flow and dike cover erosion for flood defence reliability - Literature report)

This MSc study includes a literature review of the effects of transitions on wave overtopping flow and dike cover erosion (the external erosion failure mode). It includes information on the different types of transitions and a brief description of the experimental results of the wave overtopping simulator for a number of transitions (See Figure 2). It also points to an important study (Verheij and others, 2013 and van Hoven, 2015), in which the authors quantified the effect of different types of transitions on overtopping flow (the load) and grass cover resistance (the strength).

Grass slope to grass berm. Steendam et al. (2011)

Grass slope to parking lot. Steendam et al. (2011)

Staircase on grass slope. Steendam et al. (2012)

Tree on grass berm. Steendam et al. (2011)

Fence on grass slope. Steendam et al. (2011)

Sheet pile wall with a ground sill Bakker et al. (2013)

Concrete side wall structure. Bakker et al. (2013)

Partial sheet pile wall with steel structure on top. Bakker et al. (2013)

Road on top of crest Bakker et al. (2013)

Figure Error! Use the Home tab to apply 0 to the text that you want to appear here..3: Photos of the transitions investigated with the wave overtopping simulator (van Bergeijk, 2018)

Verheij and others, 2013 and van Hoven, 2015 (Evaluation and Model Development - Grass Erosion Test at the Rhine dike)

This study is mainly based on a number of wave-overtopping experiments that were carried out in 2013 in Nijmegen and Millingen aan de Rijn (the Netherlands) to understand the failure mechanisms of grass revetments, especially near transitions and objects. Different types were investigated, namely:

■ transverse change (perpendicular to flow direction) in revetment types

■ geometrical transitions (change in landward slope inclination)

■ vertical objects and side-wall structures

The effect of transitions was quantified using 3 factors:

1. the load factor, α_M, which accounts for increase (or decrease) in load and is defined as follows:

$$\alpha_M = \frac{F_m}{F} = 1 + \frac{\mathrm{d}F}{F}$$

where F_m = shear (or normal) force in a transition case

F = shear (or normal) force in a non-transition case

dF = the increase (or decrease) in the shear (or normal) force at the transition

2. the strength factor, α_s, which accounts for reduction in strength
3. the acceleration factor α_a, which accounts for acceleration (or deceleration) that can take place due to a change in inclination (for example, acceleration due to a transition from a dike crest to landward slope)

Considering each of these in turn:

The load factor, α_M, takes into account the increase (or decrease) in shear forces. However, the limit state equations are written in terms of water velocity or flow rate. Since shear forces are a function of the square of the velocity, to apply the factor directly to velocity, we have used the square root of the factor.

The strength factor, α_s, which accounts for reduction in strength, applies to all failure modes and transition types. In a similar way to the load factor, we are using the square root when applied to limit state equations based on velocity/flow.

The acceleration factor, α_a, is based on the acceleration of the velocity (or flow) from the crest down the downstream (dry) slope based on the friction equation. Since the limit state equations are all based on the actual velocity down the back face, this coefficient is not relevant and so we have always set it to a value of 1.

Details of how these factors are quantified are given in section 5.3.

ICOLD bulletin 164, 2015 (Internal erosion of existing dams, levees and dikes, and their foundations - Volume 1: internal erosion processes and engineering assessment)

Volume 1 of this ICOLD bulletin deals with the processes and the engineering assessment of the vulnerability of a dam, levee or dike to failure or damage by internal erosion. The main mechanisms through which internal erosion is initiated are described in this volume. They are:

- concentrated leak
- backward erosion
- contact erosion
- suffusion

The overall process of erosion from initiation, through continuation of erosion, through progression, and on to breach are described for each of these mechanisms.

Based on the definition of each of these failure mechanisms, the concentrated leak mechanism was found to be the most likely to occur at the transition types covered by this study. Therefore, it was selected to simulate the failure due internal erosion at transitions and its formulation was based on section 3.3 (Criteria for initiation of concentrated leaks) of this bulletin with other relevant information in other sections. Details of this formulation is given in section 4.4.

HR Wallingford, 2019 (Transitions in flood defences – CFD study)

This study was carried out to assess the hydrodynamic performance of the overflow at the transition between a levee (grass embankment) and a flood wall (vertical wall). The main objective of the study was to quantify the relative increase of flow velocities and shear stresses at these transitions, with a particular focus on the grass embankment, which is the weaker structure. The study provides the following outputs:

- a qualitative description of flow velocity patterns and how they are influenced by the presence of transitions between a grass embankment and a vertical wall
- a quantitative estimation of the change in flow velocities due to the presence of transitions
- a quantitative estimation of the change in shear stress on the rear side of the grass embankment

These outputs were then used to quantify the load factors (described in section 6.2.2) at the following transition types:

- lower embankment (adjacent to higher vertical wall)
- higher embankment (adjacent to lower vertical wall)
- embankment and vertical wall of equal height

5. Approach

Based on the research described in section 4, the following approach was agreed with the Environment Agency:

- internal erosion at transitions to be represented by a reliability equation representing concentrated leak erosion

Note: this process will replace both of the internal erosion processes represented for the simple embankment (non-transition) scenario, that is, seepage and piping (and associated uplift). There are 2 reasons for making this change:

1. There is now an appreciation that for most UK embankments under-seepage piping, which relies on an underlying superficial permeable layer beneath the body of the embankment, is a less common risk than concentrated leak erosion, exacerbated by animal burrows and embedded objects. (There are obvious exceptions to this general rule such as the large embankments on the Thames Estuary which have underlying aquifers.) This conclusion may lead to a general change in the way that fragility curves for embankments are created in the future.
2. The nature of transitions is such that they almost always involve an abrupt permeability transition from soil to a hard material such as concrete or steel. There is a higher probability of concentrated leak erosion at this interface than elsewhere in the embankment.

- external erosion at transitions to be represented by an adjusted grass erosion reliability equation to reflect likely increases in loads on and decreases in strength of the grass to resist erosion at these locations based on its quality (for example, reduction in the case of bare patches)

The derivation of the reliability curves for each process is described in section 5 will be assumed that:

a. for water levels < embankment crest level, the failure mechanism will be internal erosion (that is, concentrated leak erosion) only
b. for water levels > embankment crest level, the failure mechanism will be a combination of internal and external erosion processes. The fragility curves for each of these processes will be combined using De Morgan's Law

Concentrated Leak Erosion Failure Mode

It is proposed that the initiation of a concentrated leak failure will be modelled using the following reliability equation:

$$z = \tau_c - \tau$$

where:

τ : Hydraulic shear stress (N/m^2) is calculated based on hydraulic load and crack type and length

τ_c : Critical shear stress (N/m^2) determined based on soil type and erodibility

Concentrated Leak Erosion is only relevant for Transition types which pass through (the majority of) the embankment structure: types 1 (embankment to wall) and 3 (embedded object). It is therefore not relevant for transition type 4 (change in surface type).

Note for readers not familiar with reliability analysis:

The reliability value z can either be negative (failed) or positive (not failed) depending on the actual magnitude of the input parameters when they are randomly sampled from across the input distributions. In the subsequent Monte Carlo simulation when this process is repeated many times, the probability of failure is then calculated as the number of instances of failure divided by the total number of instances.

This is step 5 of the overall procedure for generating fragility curves, which is as follows:

1. Identifying and analysing all relevant failure modes.
2. Identifying Limit State Equations (LSEs) or models for all failure modes (recast into reliability format: where Z (reliability) = R (strength) – S (loading)).
3. Preparing a schedule of engineering parameters (and their uncertainties).
4. Preparing fault trees specifying the logical sequence of all possible mechanisms leading to defence failure.
5. Performance of many reliability analyses for a single hydraulic loading across a range of parameter uncertainties (Monte Carlo sampling). For each loading analysed, the probability of failure is the proportion of times that Z<1. (Repeated for other hydraulic loadings and the resulting fragility curve plotted).

5.1.1 Calculating Hydraulic Shear Stress

The ICOLD bulletin 164 gives the following equations to determine hydraulic shear stress, depending on the crack shape. (Note that the hydraulic shear stress for a cylindrical crack is about half that for a vertical transverse crack.)

a. For cylindrical pipes:

$$\tau = \rho_w \frac{g H_f D}{4L}$$

b. For vertical, transverse cracks:

$$\tau = \frac{\rho_w g H_f{}^2 W}{2(H_f + W)L}$$

where:

ρ_w = Density of water in kg/m^3

g   = Acceleration due to gravity = 9.8m/s^2

H_f = Head loss in pipe or crack due to friction in metres

L   = Length of pipe or crack base in metres

D   = Diameter of the cylindrical crack in metres

W   = Width of vertical crack in metres

The hydraulic load information is collected in the same way it is collected currently in RAFT+. The shear stresses are estimated based on a series of parameters.

The ICOLD bulletin recommends crack widths of between 1 and 2mm. The shape of cracks in the body of embankments generally could be cylindrical or vertical, although the only published evidence, which relates to cracks in the surface 1.2m of embankments, suggests that the cracks are generally vertical (Dyer and others, 2009) with some horizontal cracking. Testing the impact of assuming different crack shapes and widths was carried out; the results are presented in section 7.

In the case of transitions, the hydraulic separation that may well occur at the interface between the earthen embankment and the hard structure means that vertical, transverse cracks between the flood embankment material and the hard structure are more likely. A triangular distribution of crack width between 1 and 2mm was assumed.

The following assumptions will be made regarding the crack length (of the likely crack within the embankment soil):

For type 1 (embankment to wall): Crack Length = Based on a Triangular Distribution, with the following assumptions:

- most likely length = wall width plus twice length of embedment of wall in embankment at 70% height above landside ground level
- minimum length = wall width plus twice length of wall in embankment at crest of embedment
- maximum length = wall width plus twice length of embedment of wall in embankment at landside ground level

When estimating the wall width, it is the dimension of the subsurface element that is important (not the capping beam in the case of a sheet piled wall). For sheet piling, the crack is likely to propagate along the outer face of the pans, therefore the effective 'embedded length' would be similar to a standard wall width.

The crack length would then be amended by the Condition Grade of the adjacent embankment asset.

For type 3 (embedded object): Crack Length = Full length of embedded object (or contact length), as amended by the Condition Grade of the adjacent embankment asset.

Note: Clearly, the longer the length of the crack, the smaller the shear stress (and therefore the better the reliability); so, since for this mechanism the cracks penetrate right through the structure, the wider the structure the better. Assets in worse condition are modelled with a shorter crack length to represent the reduced 'effective' width of the embankment as a result of surface defects. The amendments for the adjacent asset condition grade are given in Table 1.

Table 1: Crack length adjustments based on adjacent embankment condition grade

Condition grade of adjacent embankment	Factor applied to assumed crack length
1	1
2	1
3	0.9
4	0.5
5	0.1

The following assumptions are made regarding head loss across the crack:

For type 1 (embankment to wall): Head Loss = difference in water level between river side (level variable) and landward sides (assumed to be the downstream structure toe level or ground level).

For type 3 (embedded object): Head Loss = the difference between water level (on the waterward side) and level of bottom of the embedded object (on the landward side).

5.1.2 Calculating Critical Shear Stress

In consultation with the Environment Agency Project Executive, it was agreed that this study should not attempt to develop an approach for dispersive soils as while these are significantly more prone to erosion, their identification is highly uncertain. Dispersive soils (see Table 2) are more likely to be encountered with informal embankments, but should not occur at well-designed transition points. For this report, therefore, it has been assumed

that embankments at transitions have been designed using non-dispersive soils. However, further investigation of the extent of dispersive soils in the UK is recommended.

5.1.2.1 Note on dispersive soils

A dispersive soil is structurally unstable. In dispersive soils the soil aggregates (small clods) collapse when the soil gets wet because the individual clay particles disperse into solution. Reasons for soils being dispersive are not completely clear but may be due to the level of sodium content interfering with the structural stability of the soil.

The effect of soils being dispersive in terms of internal erosion is that they are more erodible – sometimes significantly more erodible. More information is available in the ICOLD (2016a) bulletin, in Terzaghi and others (1996) and also at department of Primary Industries and Regional Development, Australia (Department of Primary Industries and Regional Development, 2022) and identification of dispersive soils presentation (Samor, 2013). The ICOLD bulletin (ICOLD, 2016a) provides Representative Erosion Rate Indices (see Table 2).

Table 2: Representative Erosion Rate Index for Non-Dispersive Soils (ICOLD Bulletin 164)

Unified soil classification	Representative erosion rate index (I_{HET})		
	Likely minimum	Best estimate	Likely maximum
SM with <30% fines	1	<2	2.5
SM with >30% fines	<2	2 to 3	3.5
SC with <30% fines	<2	2 to 3	3.5
SC with >30% fines	2	3	4
ML	2	2 to 3	3
CL-ML	2	3	4
CL	3	3 to 4	4.5
CL-CH	3	4	5
MH	3	3 to 4	4.5
CH with liquid limit <65%	3	4	5
CH with liquid limit <65%	4	5	6

Where: SM = silty sand; SC = clayey sand; ML = silt; MH = silt of high plasticity, elastic silt; CL = clay of low plasticity, lean clay; CH = clay of high plasticity, fat clay

These Representative Erosion Rate Indices represent the following in terms of relative soil erosion rates:

Table 3: Soil erosion rates (related to Representative Erosion Rate (I_{HET}) Indices)

Representative erosion rate index (I_{HET})	Relative soil erosion rate
< 2	Extremely rapid
2 – 3	Very rapid
3 – 4	Moderately rapid
4 – 5	Moderately slow
5 – 6	Very slow
> 6	Extremely slow

Source: ICOLD Bulletin 164

The ICOLD bulletin then suggests associated critical shear stress values. Given that the whole analysis is probabilistic, we adopt a triangular distribution of assumed critical shear stress values in the analysis to get a fair representation of the uncertainties associated with allocating a particular value to a specific soil. The assumed limits and best values for the distributions are provided in Table 4:

Table 4: Limits and best estimates for a triangular distribution of critical shear stress for different soil types

I_{HET}	Critical shear stress limits for triangular distribution (Pa)		
	Low	Best	High
Up to 3	1	2	5
3.5	2	5	25
4	5	25	60
5	25	60	100

External erosion failure mode

It is proposed that initiation of external erosion at transition assets will be modelled using the following reliability equation:

$$z = \alpha_s\, q_c - \alpha_M\, \alpha_a\, q_a$$

where:

q_c = critical overtopping rate (m³/s/m), which is calculated using the Vrouwenvelder and others (2001) method, which are a parameterisation of the CIRIA 116 (Hewlett and others, 1987) curves (page 31), with adjusted coefficients (see explanation in section 5.2.1 below)

q_a = actual overtopping rate (m³/s/m), which is calculated based on the embankment geometry and wave and water level conditions (as for standard embankment assets)

α_M = the load factor, which accounts for increase in load due to the presence of the transition

α_s = the strength factor, which accounts for reduction in strength to the presence of the transition

α_a = the acceleration factor, which accounts for acceleration (or deceleration) that can take place due to a change in inclination (for example, acceleration due a transition from a dike crest to landward slope). The value of this factor in most cases is 1.0

5.2.1 Overtopping rates

The critical overtopping rate for standard embankment assets is calculated using the following equation by Vrouwenvelder and others (2001), which is, in turn, a parameterisation of the curves in CIRIA Report 116 (Hewlett and others, 1987):

$$q_c = \left[\frac{3.8 \cdot c_g^{2/3}}{(6 \cdot 10^5) 2/3 \left[1 + 0.8 \cdot \log_{10} \left(P_t \cdot t_s \cdot \frac{c_g \cdot d_w}{c_g \cdot d_w + 0.4 \cdot c_{RK} \cdot L_{K,inside}} \right) \right]} \right]^{5/2} \cdot \frac{k^{1/4}}{125 \cdot (\tan \alpha_i)^{3/4}}$$

where:

c_g = coefficient that represents the erosion endurance of the grass (ms)

P_t = percentage of the time that overtopping occurs – fixed at 100%

t_s = duration of storm (h)

d_w = the depth of the grass roots (m)

c_{RK} = coefficient with regard to the erosion endurance of the clay cover layer (ms)

$L_{k,inside}$ = width of the inside clay cover layer, that can be considered as the total width of the embankment (m)

k = roughness factor according to Strickler of the inside slope (s⁶/m²)

α_i = angle of the inside slope (°)

The values of c_g used when implementing this equation are not those associated with the CIRIA 116, because these are a conservative assessment of the original data. The original data can be found in an earlier CIRIA Technical Note 71 (Whitehead and others). We have therefore modified the c_g values that were used by a factor based on the ratio between the velocity at 1.6 hrs for TN 71 and CIRIA 116. This factor was always more than 1.0 because of the 'safety factor' embedded into the CIRIA 116 curves. The adjustment factors on c_g used were 1.42 for CG1 and CG2 (good grass), 1.29 for CG3 (medium grass) and 1.24 for CG4 and CG5 (poor grass).

There are existing relationships between erosion resistance and condition grade (see Table 5), and the erosion resistance of the transition will be altered to reflect (a) the condition grade of the adjacent embankment asset; and (b) any observed additional deterioration in the quality of the cover at the transition relative to the embankment (see section 4.3).

Table 5: Erosion strength factor (c_g) for each condition grade (HR Wallingford, 2014)

Condition grade of adjacent embankment	Grass protection on all faces	Enhanced protection on the crest	Enhanced protection on the crest and rear face	Enhanced protection on the front and rear faces and crest
1	1.42×10^6 m/s	2.14×10^6 m/s	3.20×10^6 m/s	4.28×10^6 m/s
2	1.21×10^6 m/s	1.82×10^6 m/s	2.72×10^6 m/s	3.63×10^6 m/s
3	7.71×10^5 m/s	1.16×10^6 m/s	1.74×10^6 m/s	2.31×10^6 m/s
4	5.13×10^5 m/s	7.69×10^5 m/s	1.15×10^6 m/s	1.54×10^6 m/s
5	4.08×10^5 m/s	6.12×10^5 m/s	9.17×10^5 m/s	1.22×10^6 m/s

The hydraulic load information required in the above equation will be collected in the same way it is collected at the moment in RAFT+.

The actual overtopping rates will be computed from hydraulic load information in the same way as in the existing code for standard embankment (non-transition) assets.

5.2.2 Load factors

Type 1: Embankment to wall transitions

Embankment to wall transitions were modelled in the CFD study (HR Wallingford, 2019) in order to provide an estimate of the increases in velocity and shear stress at these locations. The full document should be accessed for a complete discussion of the test method and results. However, a summary of the main outputs taken forward is provided as Appendix 1.

Although the detailed outputs from the study (see figures in Appendix) are given in terms of shear stress amplifications, it was considered more appropriate to use a velocity amplification factor to quantify the increase in the load at a transition since it is more analogous to overtopping flow which is used in the LSE for this failure mode. The HR Wallingford CFD modelling team suggested that the square root of shear stress amplifications would be representative of velocity amplifications, and these are given in Table 6. We have used triangular distributions for the amplification factors to reflect the range encountered in the CFD modelling.

Table 6: Velocity amplification factors for embankment: wall transitions

	Steep embankment (Slope:1:1 – 1:1.9) Velocity amp. factors			Shallow embankment (Slope1:2 or shallower) Velocity amp. factors		
Transition	Low	Best (use if single value only)	High	Low	Best (use if single value only)	High
Lower embankment (adjacent to higher wall)	1.00	1.14	1.26	1.00	1.18	1.34
Higher embankment (adjacent to lower wall)	1.10	1.26	1.41	1.00	1.18	1.34
Embankment and wall of equal height	1.00	1.14	1.26	1.00	1.18	1.34

Type 3: Embedded object transitions and type 4: Change in surface type

Verheij and others, 2013 and van Hoven, 2015 proposed using the following equations to quantify the increase in loads due to embedded objects:

For upstream effects: $\alpha_m = 1 + C_d/4$

For side effects: $\alpha_m = 1.4\ K_s$

Where: C_d = the drag coefficient and K_s = the shape factor. These can be determined using Figures 5.1 and table 7below.

	shape	C_D
12		1.17
13		1.20
14		1.16
15		1.60
16		1.55
17		1.55
18	vortex street	1.98
19		2.00
20		2.30
21		2.20
22		2.05

Figure Error! Use the Home tab to apply 0 to the text that you want to appear here..**4: Drag coefficients for a range of flow impact shapes (Verheij and others, 2013 and van Hoven, 2015)**

Table 7: Shape factors for a range of flow impact shapes (Verheij and others, 2013 and van Hoven, 2015

	K_s
Lenticular	0.7-0.8
Ecliptic	0.6-0.8
Circular	1.0
Rectangular	1.0-1.2
Rectangular with semi-circle nose	0.9
Rectangular with chamfered corners	1.01

Rectangular nose with wedged-shaped tail	0.86
Rectangular with sharp nose 1:2 to 1:4	0.65- 0.76

Based on the experiments carried out by Verheij and others (2013) and van Hoven (2015), it was recommended that a load factor with a triangular distribution between 1.0 and 1.7 is used for embedded structures and side walls. Therefore, values for the load factor will be adopted as shown in Table 8 with a best value of 1.5. The best value was selected based on the assumption that the load factor is likely to be closer to the upper limit value (1.7) than the lower limit value (1.0).

In the implementation in the hr*RELIABLE* tool, these factors are implemented as velocity/flow adjustment factors being the square root of the force factors.

Table 8: Load factors adopted for type 3 and type 4 transitions (for external erosion)

Transition	Low	Best (use if single value only)	High
Type 3 and type 4 transitions force factors	1.0	1.5	1.7
Type 3 and type 4 transitions velocity factors	1.0	1.23	1.30

5.2.3 Strength factors

A global strength factor at all transitions of 0.9 has been adopted based on the literature, but implemented as a critical velocity adjustment factor of the square root of this number, that is, 0.95.

5.2.4 Acceleration factors

A global acceleration factor at all transitions of 1.0 has been adopted because flow accelerations are already included in the way the limit state equation is calculated.

Adjusting the transition LSE parameters based on observed quality deficiencies

For the Concentrated Leak Erosion LSE, the assumed crack length will be automatically adjusted based on the condition of the adjacent embankment asset. It has been assumed that visual inspection cannot identify any increased risk of internal erosion, (Note that it is

possible to adjust for variations in soil type, but the visual inspection would then likely require a measure of intrusion/probing to assess this variation).

For the External Erosion LSE, the assumed erosion resistance of the clay cover will be automatically adjusted based on the difference between the general condition of the adjacent embankment and the condition immediately at the transition. Table 8 shows the proposed adjustments in condition grade that will then lead to increased probability of external erosion based on the erosion strength factors in Table 5.

If the following visual observations at a transition are made, then the condition grade should be adjusted and reflected in the selected erosion strength factors (see Table 5) by the following:

1. Good compared to the adjacent embankment (low risk of increased erosion at the transition should overtopping occur), then no change to erosion strength factor is required.
2. Showing some evidence of deterioration in quality compared to the adjacent embankment (some risk of increased erosion at the transition should overtopping occur), then the condition grade score should be reduced by 1.
3. Showing significant evidence of deterioration in quality compared to the adjacent embankment (significant risk of increased erosion at the transition should overtopping occur), then the condition grade score should be reduced by 2.

6. Concentrated Leak Erosion: non-transitions comparison with under-seepage piping fragility curves

Testing has been carried out to compare the new Concentrated Leak Erosion fragility curves, now coded within hr*RELIABLE*, with the national generic under-seepage piping fragility curves (see HR Wallingford report MCS0941-RT002-R05-00).

ICOLD bulletin 164 recommends for dams/levees of the height of typical UK levees that crack widths of between 1 and 2mm should be adopted (either cylindrical or vertical). A triangular crack width distribution with a best width of 1.5mm, minimum width of 1mm and maximum width of 2mm was therefore adopted for the comparison. Wherever applicable, the other input data was the same as that used for the original generic fragility curves.

The results are presented in Figures 6-1, 6-2, 6-3 and 6-4.
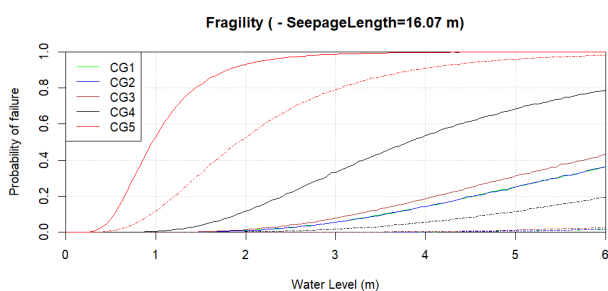
Figure Error! Use the Home tab to apply 0 to the text that you want to appear here.**.5: Narrow embankment, medium erodibility, cylindrical crack of width 1-1.5-2mm (dotted line: Transition CLE, solid line: standard embankment under-seepage)**
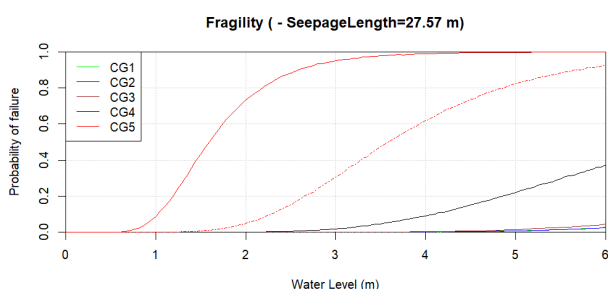
Figure Error! Use the Home tab to apply 0 to the text that you want to appear here.**.6: Wide embankment, medium erodibility, cylindrical crack of width 1-1.5-2mm (dotted line: Transition CLE, solid line: standard embankment under-seepage)**
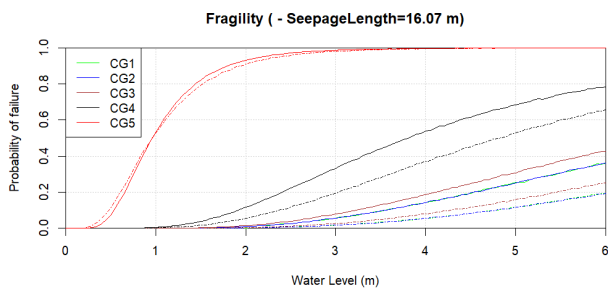
Figure Error! Use the Home tab to apply 0 to the text that you want to appear here..**7: Narrow embankment, medium erodibility, vertical crack of width 1-1.5-2mm (dotted line: Transition CLE, solid line: standard embankment under-seepage)**
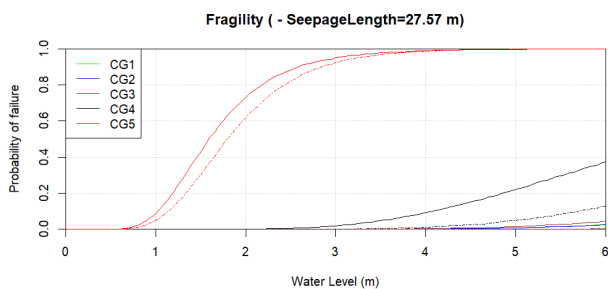
Figure Error! Use the Home tab to apply 0 to the text that you want to appear here..**8: Wide embankment, medium erodibility, vertical crack of width 1-1.5-2mm (dotted line: Transition CLE, solid line: standard embankment under-seepage**

The comparisons show that if the CLE mechanism for vertical cracks was substituted for the under-seepage piping mechanism generally (in the generic fragility curves that were used in NaFRA), the resulting fragility curves are similar enough that it would not have a big impact on the calculated flood risk. The use of vertical cracks in non-transitions situations has some justification given the work by Dyer and others (2009) (see discussion in section 5).

7. Development of the hr*RELIABLE* tool for transitions

The new reliability LSEs for transitions were incorporated into the existing hr*RELIABLE* tool using a new set of user interface web pages. The tool requires user entry of:

- a number of physical transition characteristics (transition type, soils, geometry)
- hydraulic loading conditions (water density, hydrograph characteristics, design water levels)
- on-site knowledge about transition condition

As explained in the guidance document on the transition hr*RELIABLE* tool, prepared as part of the project outputs, the tool then runs and combines the LSEs described in this report and outputs fragility curves for each transition condition grade scenario.

8. Sensitivity testing to identify transition characteristics that increase failure probabilities

Objectives of the testing

A sensitivity testing exercise was carried out looking at the impact of a range of asset and hydraulic loading characteristics on the fragility (failure vulnerability) of a particular transition, examining both the Concentrated Leak Erosion (internal erosion) and Grass Erosion (external erosion) mechanisms. The objectives of the testing were to:

■ explore the sensitivity of the annual failure probability to a number of parameters (for example, geometry, soils) using a generic hydraulic loading condition

■ evaluate the impact of a range of plausible hydraulic loading conditions on the outcomes

It was envisaged that the outcomes of the sensitivity testing would potentially:

■ support the tier 0 prioritisation process - helping to screen out transitions unlikely to pose a risk to the performance of the asset

■ in a similar way, support the tier 1 process by which transitions are selected for tier 2 evaluation

■ support the overall inspection/data collection by highlighting important information/defects to record on site; in particular, it would help define which data sets/transition characteristics should be prioritised for collection during tier 1 to support a more robust evaluation of risk using hr*RELIABLE* tool at tier 2.

Sensitivity testing methodology

There are a number of ways in which the variation of fragility curves could be quantified through sensitivity testing, but it was decided to adopt the following procedure:

■ generate the fragility curve relevant to each test

■ calculate for each fragility curve a single number, the annual failure probability by integrating the fragility curve with the distribution of extreme loadings at the site in question. This number is determined from the following relationship:

Annual p(F) = sum of (P(F) given load from fragility curve x load probability) across all loads

Having determined this basic procedure, it was then decided to carry out the sensitivity testing in 2 stages.

Stage 1 – Tidal Trent analysis. This stage examined the effect of varying each of the input parameters into the LSEs (Limit State Equations) used to generate the fragility curves. These input parameters represented the properties of the transition, either related to the strength of the transition itself or to the adjacent embankment. For this stage, to determine the annual failure probability associated with each curve, a single loading distribution representative of the Tidal Trent was used. From this analysis, the input parameters into the fragility curves which have the greatest impact on the outcome were identified.

Stage 2 – National analysis for England. Varying only those input parameters into the fragility curves having the most impact, the analysis was re-run for all transitions in England using a database of 22,919 transitions supplied by the Environment Agency, complemented by loading distribution data available from the State of the Nation analysis. Examining the data there was no general relationship between the loading distribution and the height of the defence at each transition (crest level minus ground level on the landward side of the defence). The procedure adopted therefore was as follows:

a. generate fragility curves for embankments of a range of heights and slopes incrementing in 0.1m intervals of height from 0 to 6m
b. for each of the 22,919 locations, select the fragility curve most appropriate to the height and slope of the defence (all potential slopes were examined at each location)
c. generate the annual failure probability by combining the selected fragility curve with the loading distribution relevant to that location

8.2.1 Stage 1 sensitivity analysis inputs

The inputs to generate the fragility curves for the stage 1 analysis are given for the grass erosion mechanism in table 9 and for the concentrated leak erosion mechanism in table 10.

For the Concentrated Leak Erosion mechanism, the crack lengths were calculated as follows:

■ For Type 1 transitions, the transition dimensions are as given in Figures 8-1 and 8-2. Standard deviations used for the components of the crack length were: 0.1m for L, 0.025m for W and 0.25m for X.

■ For type 3 transitions involving embedded objects, the crack length used was the length of the embedded object with standard deviation of 1.0m. For the purposes of the sensitivity analysis, it was assumed that the pipe centre line was half way up the slope.
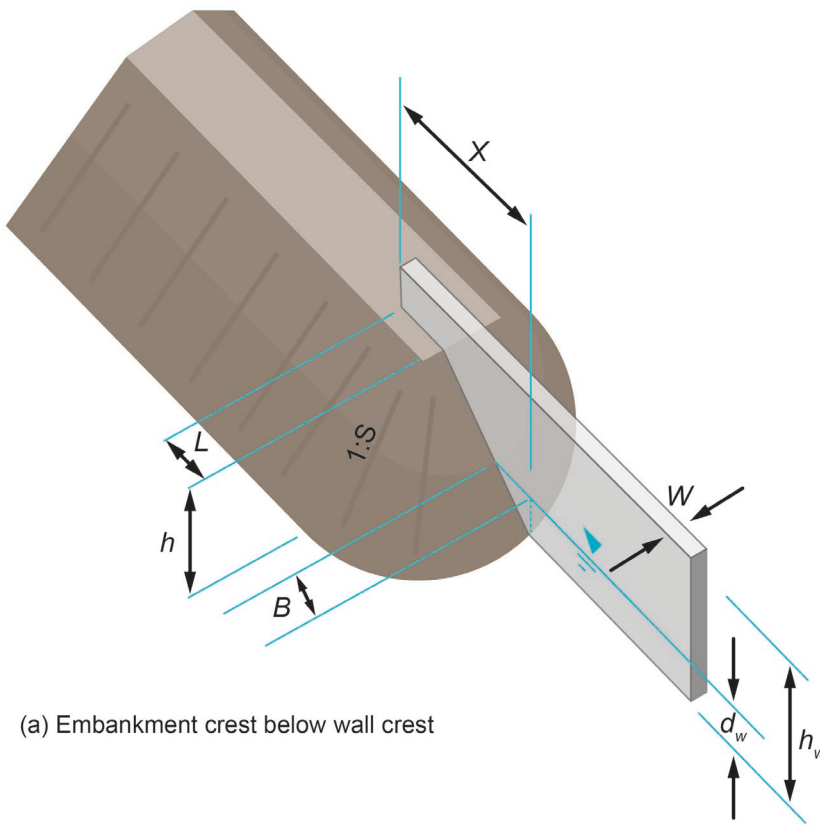
$x = L + h*S$

$B = d_w*S$

For $d_w < h$

Max seepage length = $2X + W$

Min seepage length = $2(X-B) + W$

Mid seepage length = (max + min) / 2

= $2X - B + W$

For $d_w >= h$

Max seepage length = $2X + W$

Min seepage length = $2(L) + W$

Mid seepage length = (max + min) / 2 = $X + L + W$

Where:

h_w = Wall height

(a) Embankment crest below wall crest

Figure 8 1: Main dimensions at a type 1 transition: Case (a) embankment crest below wall crest

L   = Length of wall embedded into embankment

W = Wall thickness

X = Base length of wall

h = Embankment height

S = Embankment slope

d_w = depth of water above ground level

B = See figure
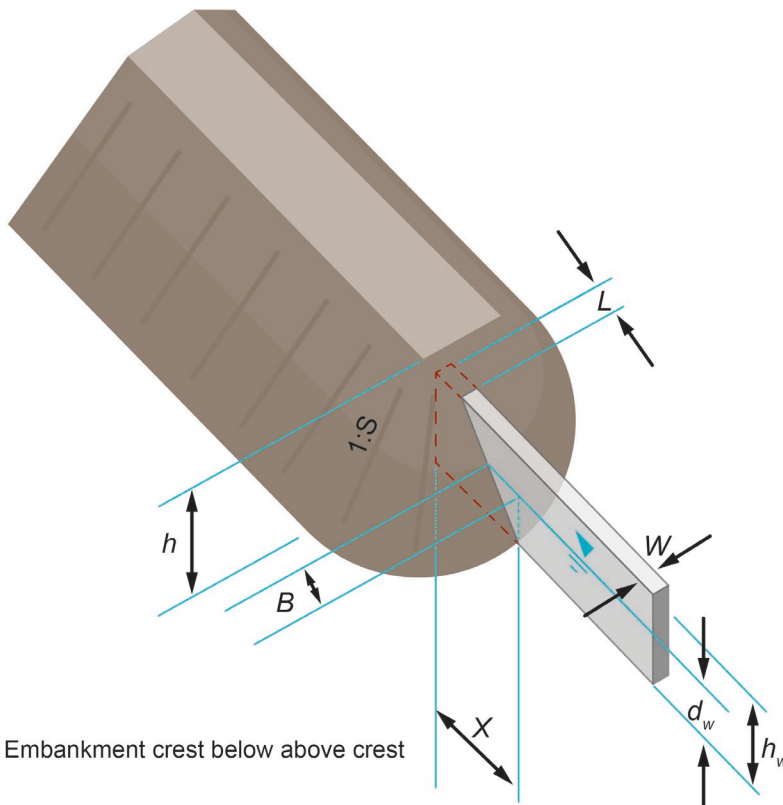
$X = L + h_w{*}S$

$B = d_w{*}S$

For dw < hw

Max seepage length = 2X +W

Min seepage length = 2(X-B) + W

Mid seepage length = (Max + Min) / 2 = 2X-B+W

For dw >= hw

Max seepage length = 2X +W

Min seepage length = 2(L) + W

Mid seepage length = (Max + Min) / 2 = X+L+W

Where:

hw = Wall height

Figure 8 2: Main dimensions at a type 1 transition: Case (b) embankment crest above wall crest

L   = Length of wall embedded into embankment

W = Wall thickness

X = Base length of wall

h = Embankment height

S = Embankment slope

dw = depth of water above ground level

B = See figure

Table 9 Sensitivity parameters for grass erosion (surface erosion)

Proposed parameters to test	Relevance for transition types	Parameter ranges for sensitivity testing	Variability
Hydrograph properties	All	Duration above crest level Baseline: Medium: 5hrs Other values: Flashy/tidal: 1.5hrs Slow: 15hrs	Medium: 2.5 to 10hrs Flashy: 0.75 to 3hrs Slow: 10 to 25hrs
Embankment crest relative to wall crest	Type 1 only	Velocity amplification	
Embankment crest relative to wall crest	Slopes <2	Levee crest higher: 1.26 Levee crest equal or lower: 1.14	1.10 to 1.41 1.00 to 1.26
Embankment crest relative to wall crest	Slopes ≥ 2	1.18	1.00 to 1.34
Landward slope	All	Baseline: 1:2 Other values: 1:1.5; 1:3; 1:5	From - 1 deg to +1 deg, except for slope 1:2 where range is from -2 deg to 0 deg
Grass quality factor by condition grade		Baseline = CG3: 0.542	

| | | CG2: 0.850 | |
| | | CG4: 0.360 | |

Table 10: Sensitivity parameters for Concentrated Leak Erosion (Internal Erosion)

Proposed parameters to test	Relevance for transition types	Parameter ranges for sensitivity testing	Variability
Water density	Type 1, type 3	Baseline: Brackish: 1,012kg/m^3 Others: Fresh: 1,000kg/m^3 Saline: 1,025kg/m^3	Brackish: SD=3kg/m^3 Fresh: SD=1kg/m^3 Saline: SD=1kg/m^3
Erosion rate index, I_{HET}, for soil type Baseline I_{HET}: 3 Other values I_{HET} = 3.5 I_{HET} = 4 I_{HET} = 5	Type 1, type 3	Equivalent critical shear stress, τ_c, for I_{HET} Baseline: τ_c = 2 Other values τ_c = 5 τ_c =25 τ_c = 60	Baseline: τ_c = 1 and 5 Other values τ_c = 2 and 25 τ_c =5 and 60 τ_c = 25 and 100
Parameters affecting crack length	Parameters affecting crack length		Variation in crack length elements given below
Embankment crest width	Type 1, type 3	Baseline: 4m Other values: 1m, 15m	
Embankment side slopes	Type 1, type 3	Baseline: 1:2 Other values: 1:1.5; 1:3; 1:5	
Embankment height	Type 1, type 3	Baseline: 1.7m (50th percentile) Other values: 0.7m (10th percentile) 1.0m (25th percentile) 2.8m (75th percentile) 3.5m (90th percentile)	

		4.5m (95th percentile)	
Seepage length by condition grade		CG3: 0.9 x crack length (baseline CG) CG2: 1.0 x crack length CG4: 0.5 x crack length	

For Concentrated Leak Erosion the following other values are used:

- gravity acceleration is 9.81m/s^2
- crack is vertical with 0.001m width
- water level in relation to crest is -5m to +10m

For grass erosion the following other values were used:

- overtopping depth = 0-1.0m (This is then converted to an equivalent overflow using the weir equation)
- grass quality for CG1 is 1424000ms (grass protection on all faces), to which the reduction factors mentioned in Table 10 are applied
- percentage overtopping during the storm duration with water above crest level = 100%
- grass root depth = 0.1m
- roughness = 0.015
- LK (width of the clay cover) = embankment width (m)
- CRK (erosion endurance of the clay cover layer) = Mean: 23,000ms and SD:100ms.

8.2.2 Inputs for the stage 2 sensitivity testing

Similar inputs were used for the fragility curves. However, as a result of further thinking about the crack width and re-evaluating the ICOLD guidance, it was decided (instead of a fixed crack width of 1mm) to adopt a triangular distribution of crack width between the 2 values provided by ICOLD of 1mm and 2mm. Therefore, a 'best value of 1.5mm was adopted, varying from a minimum of 1mm to a maximum of 2mm.

Results of the stage 1 sensitivity testing

The results of the stage 1 sensitivity testing for concentrated leak erosion are given in Table 11 for type 1 transitions and in Table 12 for type 3 transitions. Note that a ratio of 0.00 refers to scenarios where the annual probability of failure (APoF) is more than 200 times lower than the base run.

Table 10: Results for concentrated leak erosion – type 1 transitions (embankment to wall)

Variation on base run	Ratio of annual probability of failure (APoF) to APoF of base run		
	CG2	CG3	CG4
Base run (see table 10)	1	1	1
Density 1000	0.87	0.88	0.94
Density 1025	1.16	1.12	1.07
I_{HET} 3 (non-dispersive)	0.99	1.00	1.00
I_{HET} 3.5 (non-dispersive)	0.00	0.00	0.00
I_{HET} 4 (non-dispersive)	0.00	0.00	0.00
I_{HET} 5 (non-dispersive)	0.00	0.00	0.00
Slope 1.5 Height 0.7m	0.00	0.00	0.00
Slope 1.5 Height 1m	0.00	0.00	0.07
Slope 1.5 Height 1.7m	0.22	0.40	0.89
Slope 1.5 Height 2m	1.84	1.88	1.95
Slope 1.5 Height 2.8m	21.79	15.64	35.56
Slope 1.5 Height 3.5m	99.60	96.74	119.87
Slope 1.5 Height 4.5m	1193.59	878.32	253.12
Slope 2 Height 0.7m	0.00	0.00	0.00
Slope 2 Height 1m	0.00	0.00	0.04
Slope 2 Height 1.7m	0.13	0.22	0.50
Slope 2 Height 2m	0.99	0.99	1.00
Slope 2 Height 2.8m	10.39	7.05	11.74
Slope 2 Height 3.5m	34.60	26.23	54.14
Slope 2 Height 4.5m	308.92	256.26	143.31
Slope 3 Height 0.7m	0.00	0.00	0.00
Slope 3 Height 1m	0.00	0.00	0.02
Slope 3 Height 1.7m	0.05	0.10	0.19
Slope 3 Height 2m	0.42	0.41	0.36
Slope 3 Height 2.8m	3.70	2.42	1.84
Slope 3 Height 3.5m	10.09	6.25	10.78
Slope 3 Height 4.5m	36.44	31.50	39.23
Slope 4 Height 0.7m	0.00	0.00	0.00
Slope 4 Height 1m	0.00	0.00	0.01
Slope 4 Height 1.7m	0.03	0.06	0.10
Slope 4 Height 2m	0.23	0.22	0.17
Slope 4 Height 2.8m	1.85	1.16	0.55
Slope 4 Height 3.5m	4.48	2.66	2.59
Slope 4 Height 4.5m	11.87	7.47	12.25
Slope 5 Height 0.7m	0.00	0.00	0.00
Slope 5 Height 1m	0.00	0.00	0.01
Slope 5 Height 1.7m	0.02	0.04	0.06
Slope 5 Height 2m	0.15	0.13	0.09
Slope 5 Height 2.8m	1.07	0.66	0.26
Slope 5 Height 3.5m	2.43	1.43	0.75
Slope 5 Height 4.5m	5.81	3.31	4.28

Table 11: Results for concentrated leak erosion – type 3 transitions (embedded object)

Variation on base run	Ratio of annual probability of failure (APoF) to APoF of base run		
	CG2	CG3	CG4
Base run (see Table 10)	1.00	1.00	1.00
Density 1000	0.77	0.78	0.91
Density 1025	1.37	1.28	1.11
I_{HET} 3 (non-dispersive)	1.03	1.02	1.00
I_{HET} 3.5 (non-dispersive)	0.00	0.00	0.00
I_{HET} 4 (non-dispersive)	0.00	0.00	0.00
I_{HET} 5 (non-dispersive)	0.00	0.00	0.00
width 1m Slope 1.5 Height 0.7m	256.89	60.55	0.39
width 1m Slope 1.5 Height 1m	783.37	161.45	0.97
width 1m Slope 1.5 Height 1.7m	3716.08	843.24	26.65
width 1m Slope 1.5 Height 2m	7983.13	2356.04	44.23
width 1m Slope 1.5 Height 2.8m	76991.24	20159.95	92.59
width 1m Slope 1.5 Height 3.5m	235106.37	47729.42	92.59
width 1m Slope 1.5 Height 4.5m	508899.12	87684.18	92.59
width 1m Slope 2 Height 0.7m	66.26	20.45	0.29
width 1m Slope 2 Height 1m	196.55	56.50	0.64
width 1m Slope 2 Height 1.7m	747.80	212.76	11.83
width 1m Slope 2 Height 2m	1256.22	369.55	25.69
width 1m Slope 2 Height 2.8m	5553.02	2362.53	69.72
width 1m Slope 2 Height 3.5m	22118.15	8897.08	92.59
width 1m Slope 2 Height 4.5m	77170.07	24912.67	92.59
width 1m Slope 3 Height 0.7m	2.04	1.28	0.14
width 1m Slope 3 Height 1m	4.49	2.77	0.27
width 1m Slope 3 Height 1.7m	9.09	6.11	1.18
width 1m Slope 3 Height 2m	14.10	9.58	3.12
width 1m Slope 3 Height 2.8m	30.91	21.34	20.49
width 1m Slope 3 Height 3.5m	56.82	49.17	45.34
width 1m Slope 3 Height 4.5m	180.80	169.10	81.30
width 1m Slope 4 Height 0.7m	0.03	0.04	0.05
width 1m Slope 4 Height 1m	0.05	0.06	0.10
width 1m Slope 4 Height 1.7m	0.06	0.06	0.25
width 1m Slope 4 Height 2m	0.06	0.10	0.39
width 1m Slope 4 Height 2.8m	0.11	0.15	1.81
width 1m Slope 4 Height 3.5m	0.14	0.29	6.01
width 1m Slope 4 Height 4.5m	0.22	0.52	16.24
width 1m Slope 5 Height 0.7m	0.00	0.00	0.02
width 1m Slope 5 Height 1m	0.00	0.00	0.02
width 1m Slope 5 Height 1.7m	0.00	0.00	0.04
width 1m Slope 5 Height 2m	0.00	0.00	0.06
width 1m Slope 5 Height 2.8m	0.00	0.00	0.13
width 1m Slope 5 Height 3.5m	0.00	0.00	0.34
width 1m Slope 5 Height 4.5m	0.00	0.00	1.07

Variation on base run	Ratio of annual probability of failure (APoF) to APoF of base run		
	CG2	CG3	CG4
width 4m Slope 1.5 Height 0.7m	0.00	0.00	0.00
width 4m Slope 1.5 Height 1m	0.00	0.01	0.05
width 4m Slope 1.5 Height 1.7m	2.29	1.96	0.76
width 4m Slope 1.5 Height 2m	14.39	9.55	3.13
width 4m Slope 1.5 Height 2.8m	297.10	155.88	40.04
width 4m Slope 1.5 Height 3.5m	2710.59	1552.05	86.72
width 4m Slope 1.5 Height 4.5m	31741.30	13038.95	92.59
width 4m Slope 2 Height 0.7m	0.00	0.00	0.00
width 4m Slope 2 Height 1m	0.00	0.00	0.02
width 4m Slope 2 Height 1.7m	0.18	0.19	0.36
width 4m Slope 2 Height 2m	1.08	1.00	1.00
width 4m Slope 2 Height 2.8m	19.67	15.44	17.85
width 4m Slope 2 Height 3.5m	140.39	108.00	54.25
width 4m Slope 2 Height 4.5m	1506.05	1102.87	92.59
width 4m Slope 3 Height 0.7m	0.00	0.00	0.00
width 4m Slope 3 Height 1m	0.00	0.00	0.00
width 4m Slope 3 Height 1.7m	0.00	0.00	0.07
width 4m Slope 3 Height 2m	0.01	0.01	0.16
width 4m Slope 3 Height 2.8m	0.08	0.10	1.49
width 4m Slope 3 Height 3.5m	0.29	0.44	8.68
width 4m Slope 3 Height 4.5m	1.86	4.57	32.10
width 4m Slope 4 Height 0.7m	0.00	0.00	0.00
width 4m Slope 4 Height 1m	0.00	0.00	0.00
width 4m Slope 4 Height 1.7m	0.00	0.00	0.01
width 4m Slope 4 Height 2m	0.00	0.00	0.02
width 4m Slope 4 Height 2.8m	0.00	0.00	0.11
width 4m Slope 4 Height 3.5m	0.00	0.00	0.52
width 4m Slope 4 Height 4.5m	0.00	0.01	2.87
width 4m Slope 5 Height 0.7m	0.00	0.00	0.00
width 4m Slope 5 Height 1m	0.00	0.00	0.00
width 4m Slope 5 Height 1.7m	0.00	0.00	0.00
width 4m Slope 5 Height 2m	0.00	0.00	0.00
width 4m Slope 5 Height 2.8m	0.00	0.00	0.01
width 4m Slope 5 Height 3.5m	0.00	0.00	0.03
width 4m Slope 5 Height 4.5m	0.00	0.00	0.13
width 15m Slope 1.5 Height 0.7m to 2.8m	0.00	0.00	0.00
width 15m Slope 1.5 Height 3.5m	0.00	0.00	0.08
width 15m Slope 1.5 Height 4.5m	0.00	0.02	3.38
width 15m Slope 2 Heights 0.7m to 2.8m	0.00	0.00	0.00
width 15m Slope 2 Height 3.5m	0.00	0.00	0.02
width 15m Slope 2 Height 4.5m	0.00	0.00	0.76

Variation on base run	Ratio of annual probability of failure (APoF) to APoF of base run		
	CG2	CG3	CG4
width 15m Slope 3 Height 0.7m to 3.5m	0.00	0.00	0.00
width 15m Slope 3 Height 4.5m	0.00	0.00	0.03
width 15m Slope 3 Height 0.7m to 3.5m	0.00	0.00	0.00
width 15m Slope 3 Height 4.5m	0.00	0.00	0.03
width 15m Slope 4 Height 0.7m to 4.5m	0.00	0.00	0.00
width 15m Slope 4 Height 0.7m to 4.5m	0.00	0.00	0.00

Note: All the results presented in Table 11 and Table 12 are for non-dispersive soils. The extent of dispersive soils in flood embankments in England is currently unknown and for I_{HET} of 3.5 or greater they have very little impact on concentrated leak erosion. However, for the base case of I_{HET} of 3.0, analysis showed that the annual failure probability via concentrated leak erosion would increase by 2 orders of magnitude if the soils were dispersive rather than non-dispersive.

Reviewing Table 11 and Table 12, it can be inferred that any prioritisation of attention regarding concentrated leak erosion at transitions should focus on embankments with:

■ heights greater than or equal to 2 metres

■ slopes of 1:3 or steeper

■ crest widths of 4m or less ('narrow' rather than 'wide' embankments)

The results of the stage 1 sensitivity testing for grass erosion are given in Table 13 for type 1 transitions and in Table 14 for type 3 transitions.

Table 12: Results for grass erosion – type 1 transitions (embankment to wall)

Variation on base run	Ratio of annual probability of failure (APoF) to APoF of base run		
	CG2	CG3	CG4
Base run (slope 1:2, duration 5hrs)	1.00	1.00	1.00
Slope 1.5	1.37	1.29	1.06
Slope 3	0.63	0.72	0.79
Slope 4	0.38	0.59	0.66
Slope 5	0.27	0.48	0.62
Duration 15 hrs	1.97	1.62	1.23
Duration 1.5 hrs	0.13	0.37	0.45

Table 13: Results for grass erosion – type 4 transitions (change in embankment revetment/surface covering)

Variation on base run	Ratio of annual probability of failure (APoF) to APoF of base run		
	CG2	CG3	CG4
Base run (slope 1:2, duration 5hrs)	1.00	1.00	1.00
Slope 1.5	1.55	1.30	1.10
Slope 3	0.73	0.79	0.82
Slope 4	0.47	0.61	0.68
Slope 5	0.34	0.49	0.59
Duration 15 hrs	2.12	1.64	1.18
Duration 1.5 hrs	0.18	0.38	0.47

Reviewing Table 13 and Table 14, it can be inferred that any prioritisation of attention to transitions from the perspective of rear face grass erosion should focus on embankments with steeper rear slopes and subject to longer periods of overflow. Unlike with concentrated leak erosion, the analysis does not reveal any really clear-cut thresholds above which most focus should be given. However, if the focus is kept on embankments with rear slopes of 1:3 or steeper (as adopted for concentrated leak erosion), this will also cover those embankments most vulnerable to grass erosion.

A supplementary piece of work was also carried out to evaluate the effect of local crest level reductions (due to settlement, trampling) on increasing the annual failure probability due to external rear face grass erosion. The broad conclusions of this analysis were as follows:

- The annual failure probabilities associated with external rear face grass erosion for the base run are 2 orders of magnitude smaller than those associated with concentrated leak erosion. This is primarily because the probabilities associated with concentrated leak erosion have a much high proportion of the loading distribution associated with them.
- The annual failure probabilities (see Table 15) for rear face grass erosion:
  - remain one order of magnitude less than those for concentrated leak erosion with local crest level reductions up to 0.3m
  - only reach the same order of magnitude as those for concentrated leak erosion when crest level reductions exceed 0.6m, which would be exceptional

Table 14 Effect on annual failure probability of local crest level reductions

Annual failure probability for	CG2	CG3	CG4
Base run	0.016%	0.031%	0.045%
crest level reduction = 0.1m	0.051%	0.085%	0.107%
crest level reduction = 0.2m	0.112%	0.159%	0.189%
crest level reduction = 0.3m	0.200%	0.269%	0.313%
crest level reduction = 0.4m	0.325%	0.424%	0.488%
crest level reduction = 0.5m	0.511%	0.663%	0.761%
crest level reduction = 0.6m	0.785%	1.002%	1.138%
crest level reduction = 0.7m	1.184%	1.498%	1.738%
crest level reduction = 0.8m	1.824%	2.669%	3.606%

Results of the stage 2 sensitivity testing

The results of the national scale analysis across England across all 23,976 transition assets are presented in Table 16 to Table 20, with embankment side slope assumptions for each table ranging from 1:1.5 (Table 16) to 1:5 (Table 20). Unsurprisingly, the highest probabilities of failure are associated with the steepest side slopes. To understand the data for prioritisation purposes, the focus has been on situations where at least 99% of the annual failure probabilities are less than 5% (0.05), which is typically taken as a maximum allowable annual failure probability. From the tables, we may conclude that the focus should be on the following situations:

- for embankments with side slopes 1:1.5, those embankments of height greater than 1.75m
- for embankments with side slopes 1:2, those embankments of height greater than 2.0m
- for embankments with side slopes 1:3, those embankments of height greater than 3.0m
- for embankments with side slopes 1:4, those embankments of height greater than 4.0m
- for embankments with side slopes 1:5, those embankments of height greater than 5.0m

From this, it is apparent that the conclusion from the Tidal Trent area analysis that only transition assets with embankment heights (crest level minus landward ground level) greater than or equal to 2 metres need be prioritised at tier 0 for inspection and investigation is broadly supported. This simplified conclusion is cautious, but does reflect the considerable uncertainty about the actual side slopes of many of English embankments.

Table 15: Distribution of annual probability of failure assuming side slopes of 1:1.5

Annual prob. of failure	Height (m)									
	1	1.25	1.5	1.75	2	3	4	5	10	15
Up to 0.01	7,272	1,778	2,138	1,273	2,001	2,813	1,119	447	391	56
Up to 0.02	23	43	107	60	122	207	106	33	6	0
Up to 0.03	11	13	85	43	83	144	49	25	3	0
Up to 0.04	3	7	33	53	37	96	49	16	5	0
Up to 0.05	3	1	8	52	45	91	33	16	2	0
Up to 0.1	1	3	6	78	152	306	131	56	14	0
Up to 0.15	0	0	1	5	90	385	206	34	36	0
Up to 0.2	0	0	0	0	0	237	139	44	11	0
Up to 0.25	1	0	0	0	0	167	90	36	17	0
Up to 0.3	0	0	0	0	0	66	106	19	25	0
Up to 0.4	0	0	0	0	0	7	81	30	4	0
Up to 0.5	0	0	0	0	0	0	54	25	9	0
Up to 0.75	0	0	0	0	0	0	33	17	5	0
Up to 0.9	0	0	0	0	0	0	22	15	4	0
Up to 1	0	0	0	0	0	0	2	60	126	19
% total ≤ 0.05	100.0	100.0	100.0	99.7	96.4	80.9	67.0	67.9	64.0	74.7

Table 16: Distribution of annual probability of failure assuming side slopes of 1:2

Annual prob. of failure	Height (m)									
	1	1.25	1.5	1.75	2	3	4	5	10	15
Up to 0.01	7,282	1,807	2,228	1,331	2,164	4,212	1,895	714	520	56
Up to 0.02	17	22	121	86	101	221	92	26	8	0
Up to 0.03	8	11	18	90	56	68	59	27	11	0
Up to 0.04	3	2	8	38	57	16	52	17	8	1
Up to 0.05	2	2	2	8	46	2	42	10	10	1
Up to 0.1	1	1	1	11	101	0	79	36	32	0
Up to 0.15	0	0	0	0	5	0	1	37	28	3
Up to 0.2	1	0	0	0	0	0	0	6	9	1
Up to 0.25	0	0	0	0	0	0	0	0	6	0
Up to 0.3	0	0	0	0	0	0	0	0	4	0
Up to 0.4	0	0	0	0	0	0	0	0	5	0
Up to 0.5	0	0	0	0	0	0	0	0	6	1
Up to 0.75	0	0	0	0	0	0	0	0	8	1
Up to 0.9	0	0	0	0	0	0	0	0	3	2
Up to 1	0	0	0	0	0	0	0	0	0	9
% total ≤ 0.05	100.0	100.0	100.0	100.0	99.8	89.2	78.7	76.2	72.3	74.7

Table 17: Distribution of annual probability of failure assuming side slopes of 1:3

Annual prob. of failure	Height (m)									
	1	1.25	1.5	1.75	2	3	4	5	10	15
Up to 0.01	7,290	1,824	2,345	1,477	2,320	3,654	1,603	644	479	56
Up to 0.02	16	15	28	76	146	213	134	40	25	0
Up to 0.03	3	4	3	8	50	114	78	19	9	0
Up to 0.04	3	1	1	1	9	156	63	12	9	0
Up to 0.05	1	1	0	0	5	91	41	10	6	0
Up to 0.1	0	0	1	2	0	268	142	55	19	2
Up to 0.15	0	0	0	0	0	23	151	41	45	0
Up to 0.2	1	0	0	0	0	0	8	41	22	3
Up to 0.25	0	0	0	0	0	0	0	11	10	1
Up to 0.3	0	0	0	0	0	0	0	0	4	0
Up to 0.4	0	0	0	0	0	0	0	0	5	0
Up to 0.5	0	0	0	0	0	0	0	0	4	0
Up to 0.75	0	0	0	0	0	0	0	0	4	0
Up to 0.9	0	0	0	0	0	0	0	0	6	1
Up to 1	0	0	0	0	0	0	0	0	11	12
% total ≤ 0.05	100.0	100.0	100.0	100.0	100.0	99.5	92.8	89.3	83.1	77.3

Table 18: Distribution of annual probability of failure assuming side slopes of 1:4

Annual prob. of failure	Height (m)									
	1	1.25	1.5	1.75	2	3	4	5	10	15
Up to 0.01	7,295	1,835	2,368	1,553	2,474	3,905	1,837	714	526	56
Up to 0.02	12	7	9	9	52	284	112	24	20	2
Up to 0.03	4	2	0	0	3	182	64	29	5	0
Up to 0.04	2	1	1	0	1	96	40	17	18	0
Up to 0.05	0	0	0	2	0	46	44	14	9	1
Up to 0.1	0	0	0	0	0	6	122	41	33	3
Up to 0.15	1	0	0	0	0	0	1	34	14	0
Up to 0.2	0	0	0	0	0	0	0	0	13	0
Up to 0.25	0	0	0	0	0	0	0	0	6	2
Up to 0.3	0	0	0	0	0	0	0	0	13	2
Up to 0.4	0	0	0	0	0	0	0	0	1	5
Up to 0.5	0	0	0	0	0	0	0	0	0	4
Up to 0.75	0	0	0	0	0	0	0	0	0	0
Up to 0.9	0	0	0	0	0	0	0	0	0	0
Up to 1	0	0	0	0	0	0	0	0	0	0
% total ≤ 0.05	100.0	100.0	100.0	100.0	100.0	100.0	100.0	96.1	92.9	82.7

Table 19: Distribution of annual probability of failure assuming side slopes of 1:5

Annual prob. of failure	Height (m)									
	1	1.25	1.5	1.75	2	3	4	5	10	15
Up to 0.01	7,298	1,838	2,374	1,562	2,520	4,173	1,970	758	562	58
Up to 0.02	10	6	3	0	9	285	87	37	23	3
Up to 0.03	4	1	1	0	1	57	82	17	16	1
Up to 0.04	1	0	0	2	0	4	58	11	5	0
Up to 0.05	0	0	0	0	0	0	16	13	7	0
Up to 0.1	0	0	0	0	0	0	7	37	12	0
Up to 0.15	1	0	0	0	0	0	0	0	19	2
Up to 0.2	0	0	0	0	0	0	0	0	14	6
Up to 0.25	0	0	0	0	0	0	0	0	0	5
Up to 0.3	0	0	0	0	0	0	0	0	0	0
Up to 0.4	0	0	0	0	0	0	0	0	0	0
Up to 0.5	0	0	0	0	0	0	0	0	0	0
Up to 0.75	0	0	0	0	0	0	0	0	0	0
Up to 0.9	0	0	0	0	0	0	0	0	0	0
Up to 1	0	0	0	0	0	0	0	0	0	0
% total ≤ 0.05	100.0	100.0	100.0	100.0	100.0	100.0	100.0	100.0	95.0	82.7

Conclusions

8.5.1 For the tier 0 prioritisation process

Since, of the required data at tier 0 (height, side slope, crest width), the AIMS database only consistently contains height data, it is only possible to add the criterion to the tier 0 prioritisation that embankment heights (crest level minus landward ground level) for

assessment of transitions should be 2 metres high or greater. However, ruling out embankments of less than 2.0m height or less is a significant saving, since these represent some 60% of all the embankments in England (14,245 assets out of 23,976).

8.5.2 For tier 1 identifying transitions for tier 2 evaluation

For the tier 2 evaluation, in addition to the requirement that embankment height (crest level minus landward ground level) should be greater than 2 metres for further investigation, the following additional criteria can be used to screen out transitions that merit further evaluation:

- With respect to embankment side slopes and heights:
  - for embankments with side slopes 1:3: embankments of height 3.0m or less
  - for embankments with side slopes 1:4: embankments of height 4.0m or less
  - for embankments with side slopes 1:5: embankments of height 5.0m or less
- Any embankment with a crest width of greater than 4m ('wide' rather than 'narrow' embankments)
- Any embankment with soils with I_{HET} greater than 3.0
- Local crest settlements of 0.3m or less

Therefore, during the tier 1 inspection it is highly desirable to collect data, if it is not already available locally, on the embankment crest width and side slopes. This is in addition to the measurements required at the transition itself in order to estimate crack length. Information from boreholes or elsewhere should also be sourced to identify the soil type used in the embankment from which an estimate of I_{HET} can be made.

In theory, these quantified screening thresholds could be applied at tier 0, where suitable data sets are available. For example, processed LiDAR data on embankment crest widths and side slopes could be used, although the suitability/accuracy of the data might need to be explored.

8.5.3 Understanding the extent and role of dispersive soils

For soils with an I_{HET} greater than 3.0, the effect on erodibility of them being dispersive appears to be small. However, a trial use of I_{HET} values of 3.0 or less, reflecting dispersive soils rather than non-dispersive, (which was not part of the main sensitivity analysis) showed that the annual failure probability via concentrated leak erosion would increase by 2 orders of magnitude. This is likely to be significant because such low I_{HET} values could apply to a broad range of soils in the UK, including to silty and clayey sands and to any silts and clays of low plasticity. At the moment, we simply do not know the extent of use of such soils in flood embankments and, assuming they are used, the extent to which these soils may be dispersive. Given the large potential impact of dispersive soils a national survey should be considered to identify their presence and quantify their impact.

9. References

DYER, M., UTILI, S. AND ZIELINSKI, M., 2009. Field survey of desiccation fissuring of flood embankments. Proc. Instn. Civ. Engrs – Wat. Mgt. WM3, 221-232.

DEPARTMENT OF PRIMARY INDUSTRIES AND REGIONAL DEVELOPMENT., 2022. Identifying dispersive (sodic) soils. Accessed on 26th October 2022 from: https://www.agric.wa.gov.au/dispersive-and-sodic-soils/identifying-dispersive-sodic-soils

ICOLD, 2016a. Internal erosion of existing dams, levees and dikes and their foundations. Bulletin 164. Volume 1: Internal erosion processes and engineering assessment. Paris: ICOLD.

ICOLD, 2016b. Internal erosion of existing dams, levees and dikes and their foundations. Bulletin 164. Volume 2: case histories, investigations, testing, remediation and surveillance. Paris: ICOLD.

HEWLETT, H., BOORMAN, L. AND BRAMLEY, M., 1987. Design of reinforced grass waterways. CIRIA report 116. London: CIRIA.

HR WALLINGFORD, 2014. Improved generic fragility curves for use in flood risk analysis, Wallingford: HR Wallingford. Report MCS0941-RT002-R05.

HR WALLINGFORD, 2019. Transitions in Flood Defences - CFD study, (MCR5953-RT004-R01-00).

SAMOR, R. 2013. Identification of dispersive soils. Accessed on 26th October 2022 from: https://www.slideshare.net/rizwansamor/identification-of-dispersive-soils

TERZGAGHI, K., PECK, R.B. AND MESRI, G.,1996. Soil Mechanics in Engineering Practice, 3rd Edition, New York: Wiley Interscience.

VAN BERGEIJK, V.M., 2018. The effects of transitions on wave overtopping flow and dike cover.

VERHEIJ, H., HOFFMANS, G. AND VAN DER MEER, J., 2013. Evaluation and Model Development Grass Erosion Test at the Rhine dike (release 1). Delft: Deltares.

VERHEIJ, H., HOFFMANS, G., VAN DER MEER, J. AND VAN HOVEN, A., 2015. Evaluation and Model Development Grass Erosion Test at the Rhine dike (release 4). Delft: Deltares.

VROUWENVELDER, A.C.W.M., STEENBERGEN, H.M.G.M. AND SLIJKHUIS, K.A.H., 2001. Theoretical manual of PC-Ring, Part A: descriptions of failure modes (in Dutch), Nr. 98-CON-R1430, Delft.

WHITEHEAD, E. AND NICKERSONS OF ROTHWELL, 1976. A guide to the use of grass in hydraulic engineering practice. CIRIA Technical Note 71. London: CIRIA.

10. Appendices

10.1 CFD modelling (HR Wallingford, 2019)

This appendix presents the CFD modelling work. Results were presented in terms of velocity amplifications and shear stress amplifications. The amplification of the shear stress at the transitions was calculated in comparison with the level of shear stresses at the main trunk of the overflowed structure. Model results suggest that there is an amplification of shear stress of ~1.5 to 2 times in most cases.

The results from the CFD model provide an initial estimate of the overall level of shear stress amplification in these transitions. This amplification factor is then used directly in calculating sheer stress due to overtopping at transition points. As with all modelling work, there are a set of assumptions/limitation to this work and these are set out in Section 10.3.5. In particular, where a transition has significantly different geometry from that modelled, there is much greater potential for the amplification factor to be outside the range stated.

10.2 Study objectives

A CFD model of a typical channel was built in order to assess the hydrodynamic performance of the overflow at the transition between a levee (grass embankment) and a flood wall (vertical wall). The main objectives of the study were to assess the relative increase of flow velocities and shear stresses at these transitions, with particular interest in the grass embankment, which is the 'weaker' structure.

The CFD study will provide:

- a qualitative description of how flow velocity patterns are influenced by the presence of transitions between a grass embankment and a vertical wall
- a quantitative estimation of the change in flow velocities due to the presence of transitions
- a quantitative estimation of the change in shear stress above the rear side of the grass embankment

This report is organised as follows: the model set-up is described in section 2, the test programme is presented in section 3, modelling results are reported in section 4 and the report is concluded in section 5.

10.3 Model set-up

10.3.1 CFD model

The CFD simulations were performed using the OpenFOAM® software package (www.openfoam.com), which is a world-class, general purpose, open-source CFD software, licensed under the GNU General Public License, capable of modelling (among other processes):

1. steady-state and transient flows

2. laminar and turbulent flows

3. multiphase flow (free-surface)

HR Wallingford maintains its own version of OpenFOAM® software, which has been extensively validated for 3D flow and interaction with hydraulic structures within the framework of the internal research project CAY0457: OpenFOAM®-CFD Facility (HR Wallingford 2014).

10.3.2 Model geometry

A sketch of the modelled geometry is presented in Figure 10.1. We will consider 4 transitions in the same model, as shown below. Note that the height of each element is defined as the distance between the channel bed and its crest:

- T1: From an embankment 2.5m high to a lower flood wall 2.2m high
- T3: From a wall 2.2m high to a higher embankment 2.5m high
- T2: From a wall 3.5m high, to a lower embankment 2.20m high
- T4: From an embankment, 2.20m high, to a higher wall 3.5m high
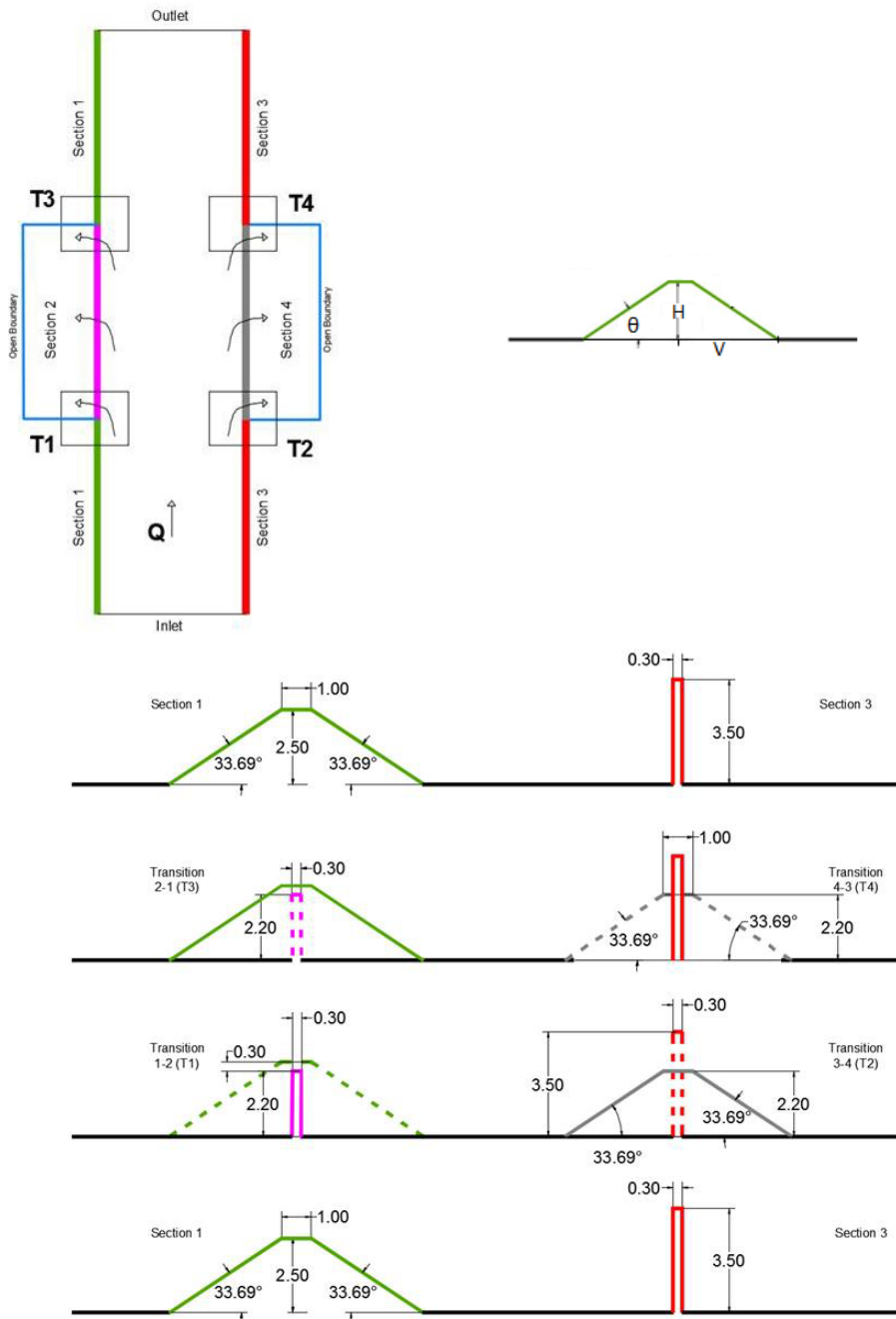
Figure 10.1: Sketch of the model geometry with typical dimensions and slopes

Two slopes (Geometry 01 and Geometry 02) of the embankment will be considered:

- **Geometry 01** → 1 V: 1.5 H or $\theta = 33.69°$
- **Geometry 02** → 1 V: 2.5 H or $\theta = 21.80°$

Embankments with wide crests (for example, > 1m) have, in general, a lower probability of failure and, therefore, a narrow embankment with a crest width of 1m is considered in this

study. The width of the vertical wall is considered to be 0.30m. The width of the channel is 50m wide enough so there is no interference between the flow of both banks.

A sketch of the numerical model domain for Case 01 is presented in Figure 10.2. The transition between the vertical wall and the embankment is considered to be rounded, as shown in Figure 10.3. The channel slope is assumed to be 1:1000 or 0.1%. This is an average value obtained from the slopes of several UK rivers (Samuels, 1989). Effective surface roughness coefficients K_s considered for the different elements of the model, river bed, grass embankments and vertical walls, are presented in Figure 10.4.
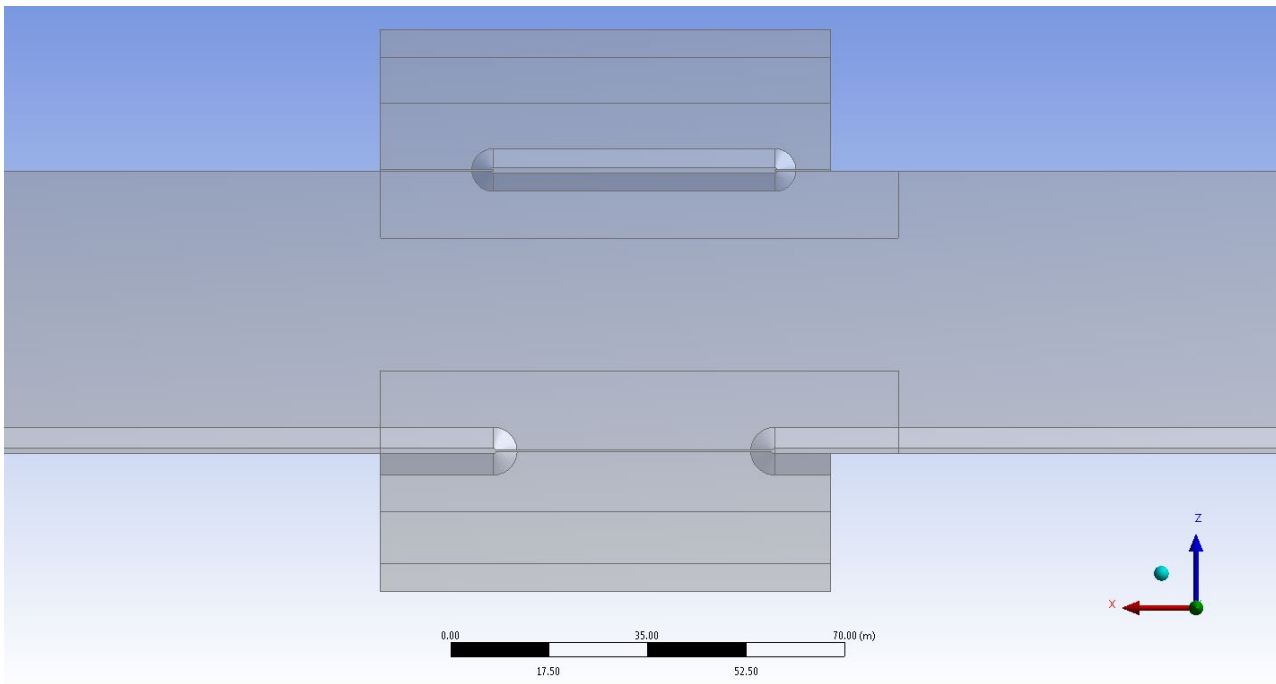
Figure 10.2: Case 01- Numerical model domain
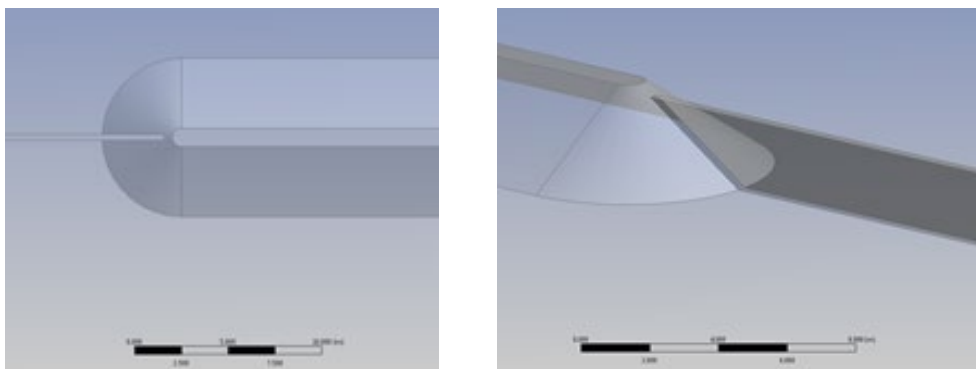
Figure 10.3: Transition: Top (left) and 3D (right) view
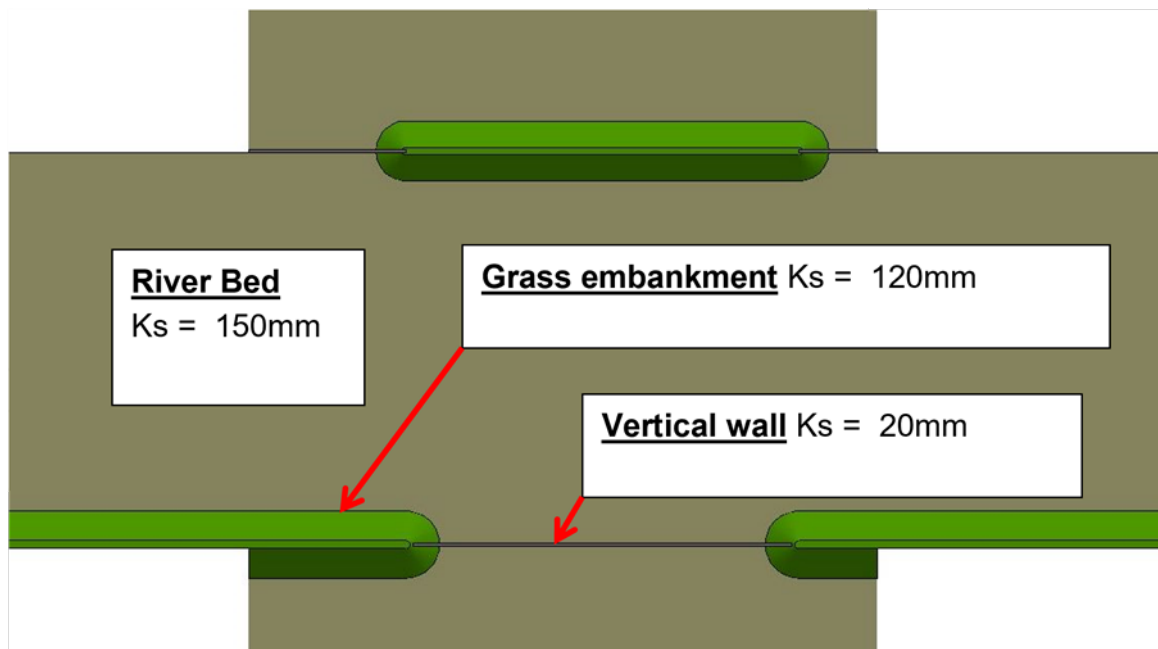
Figure 10.4: Effective surface roughness coefficients Ks. Grass embankments are shown with green colour

10.3.3 Mesh

The model mesh is generated using snappyHexMesh, the built-in OpenFOAM mesher. A single mesh configuration was tested for each case having a uniform background mesh resolution with the default characteristic edge length of 0.5m. Mesh refinements were applied at both grass embankment and vertical wall (up to 0.125m), in in the vicinity of the transitions (up to 0.0625m) where higher resolution was considered a requirement. The mesh size was refined to 0.25m in all remaining domains. Mesh refinement was relaxed to 0.5m toward the top boundary and the outlets. Example snapshots of the model mesh for one of the test cases showing refinement areas are presented in Figure 10.5. The mesh arrangements in general have an overall number of cells of approximately 5 million.
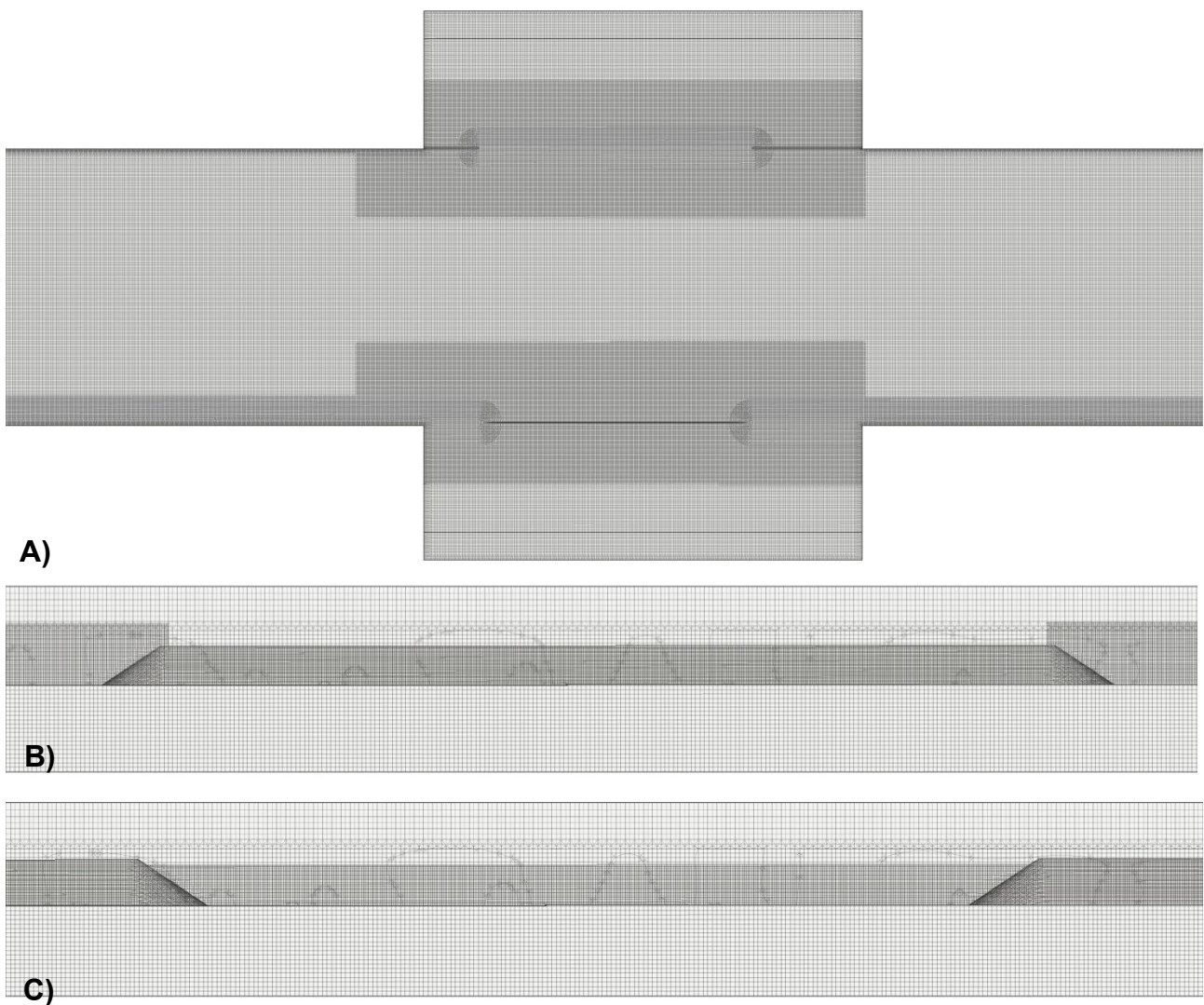
Figure 10.5: Numerical model mesh for the Case 01 - Plan view (A), Lateral view of the flood defences (B-Embankment, C-Vertical wall)

10.3.4 Physics set-up

The simulations are set up for 2-phase flow: water and air. The water and air densities are set to 1,000.73kg/m^3 and 1kg/m^3, respectively, and their kinematic viscosities to 1.29x10^{-6}m^2/s and 1.48x10^{-5}m^2/s respectively. Turbulence properties were taken into account by using the k-omega Shear Stress Transport (SST) turbulent closure model.

10.3.5 Boundary conditions

The following boundary conditions were assigned to the domain boundaries:

- At the upstream inlet, a constant flow discharge is applied. The water level is adjusted according to the local flow conditions.

- At the 2 side outlets, constant water depth is imposed using the relaxation zone technique.

- At the downstream outlet water depth is imposed using the relaxation zone technique.

- At the top boundary (atmosphere) a constant pressure head for the air phase is imposed. Water and air volumes were permitted to exit the domain where required. Only air volumes were allowed to enter from this boundary. Turbulent characteristics were calculated locally by the model solution.

- The remaining boundaries are treated as solid walls. No-slip condition is enforced coupled with turbulent wall functions for calculating near-wall turbulent characteristics, including the effect of roughness.

Sketches showing the boundary conditions used and their locations are presented in Figure 10.6.

Atmosphere:

Constant pressure head

Flood defences and bed:

Solid no-slip condition

Outlet:

Fixed water depth

Inlet:

Imposed constant discharge and a variable water depth
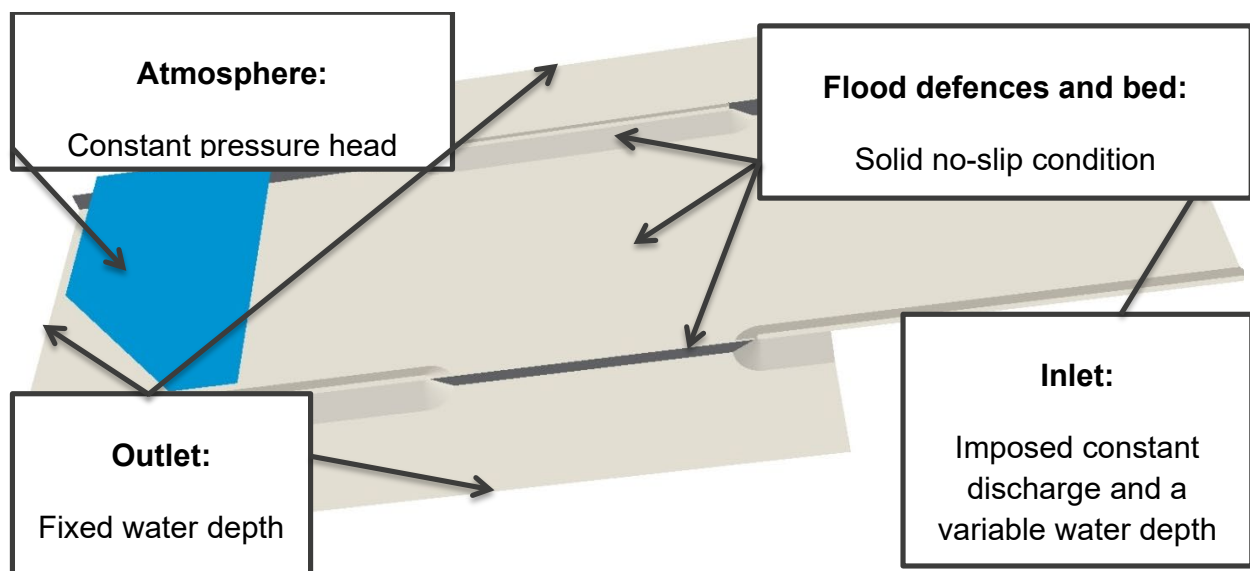
Figure 10.6: Boundary conditions of computational domain

10.3.6 Test programme

A total of 4 test scenarios were considered as described in Table 10.1. The test conditions selected were intended to cover 2 representative overflowing events for each of the geometry considered (see section 10.3.2). Overflow heights were set to ~250mm and ~125mm. Values were set at the upstream edge of each transition, but in the course of

simulations, water level at the overflowing part was close to, but not exactly at, these values, as the local evolution of velocities and shear stresses will change the water level along the overflowing part of the transition.

Both scenarios were associated to typical velocity values. During flood events in the UK rivers vary largely depending on geometric parameters such as channel slope or cross-section and hydrometric parameters such as the amount of rainfall and run-off. Empirical equations nevertheless provide simple estimations of flow velocities based on channel discharge only. Based on an analysis of 2 different equations presented in Lewin (1981), a flow velocity of 1.5m/s is considered representative of flood conditions. Flow conditions in the model must be prescribed in terms of upstream flow discharge and downstream water level. Several trial and error attempts were made to ensure that overflow height matched the values intended.

Every simulation was run for 500s of model time, using a variable time-step for the time advancement algorithm. The flow variables were monitored in time and to ensure that the model reaches beyond spin-up phase. Indicative water velocity time series are shown in Figure 10.7 for Case 02 and Case 03. Time series were sampled at the points shown in Figure 10.8, demonstrating that simulations reached a quasi-steady state.

Table 10.1: Test cases-flow condition

Test case	W.L. [m] Downstream	Q [m³/s] Upstream	W.L. [m] Above transitions
01	2.314	172	0.250
02	2.350	155	0.250
03	2.255	160	0.125
04	2.287	148	0.125
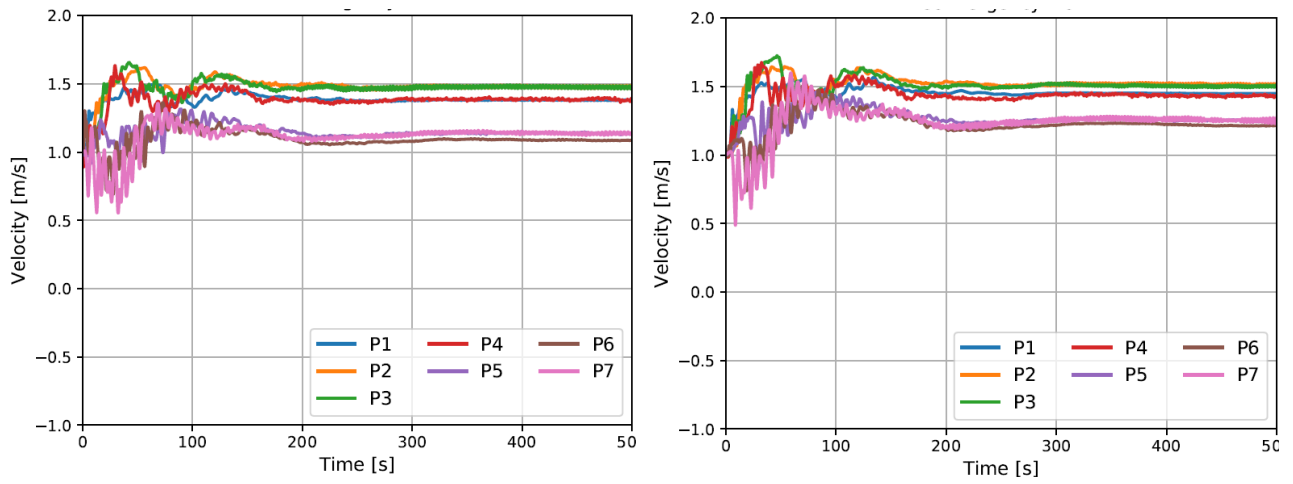
Figure 10.7: Flow velocity (magnitude) for Case 02 (left) and Case 03 (right)
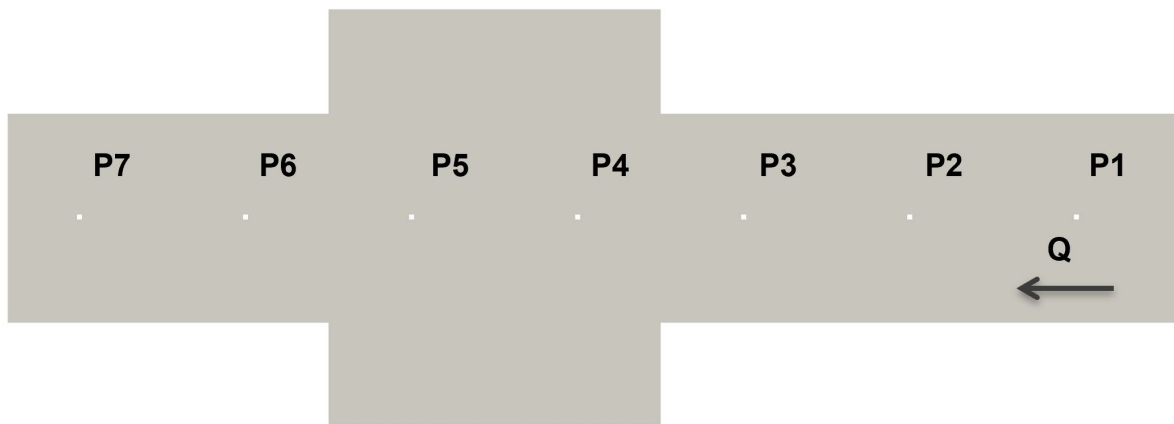
Figure 10.8: Intake structure C - Position of probes

10.4 Results

10.4.1 Sampling locations

Main flow variables were visualised at the planes shown in Figure 10.9 and Figure 10.10. Illustrative flow velocity distributions and amplification factor referring to the upstream value (1.5m/s) for velocity are reported for the domain and for 2 longitudinal cross sections (S1 and S2) indicated in Figure 10.9. The reference segment (R in Figure 10.10) was selected to show the pattern of shear stress along the central zone of the lower embankment and to evaluate an average value for each layer shown in Figure 10.10. A normalised shear stress value was calculated for the 4 roundheads at transitions. Normalised values at each elevation were calculated with respect to the average values, and results are shown for views V1, V2, V3 and V4 (Figure 10.9).

Note that the CFD model we used is a 2-phase model which calculates the percentage of water within a cell. It is subject to simplifying assumptions with respect to the evolution of local flow patterns, especially if these are expected to be shallow. Aerated areas are also approximated, as the CFD model does not have the capacity to solve for bubbles or splashes smaller than ~10cm due to the practical limitations imposed by the mesh refinement and computational burden. The shear stress output is shown only at the locations which are assumed to be wet. In this case, we assumed that 'wet' mesh cells are the ones > 10%, and we assigned water density for them for calculating shear stress.
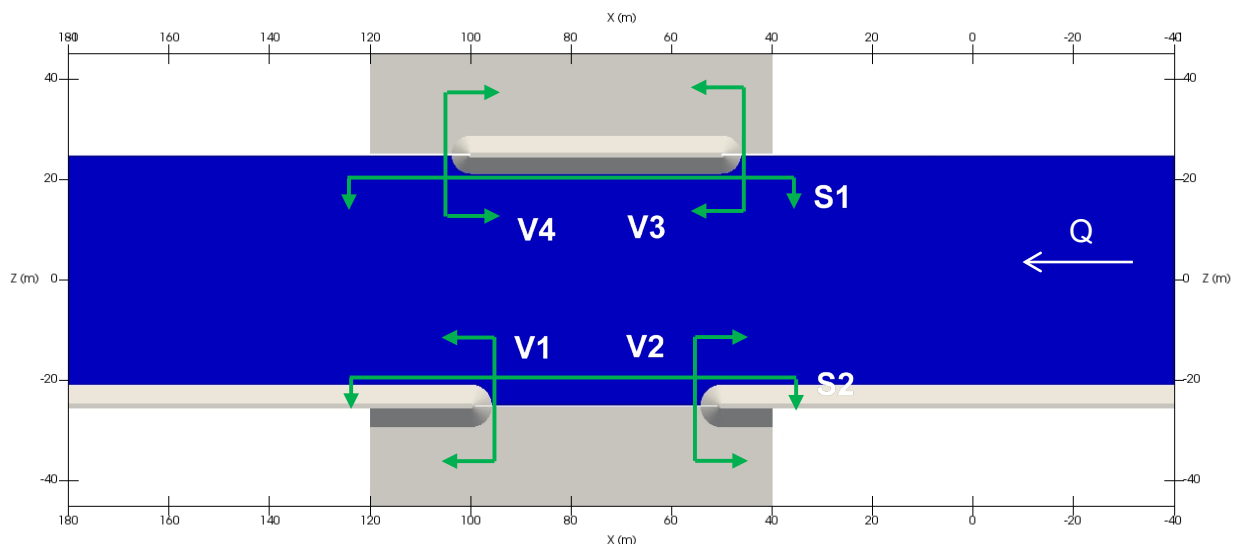
Figure 10.9: Reference views (V) and sections (S) for visualisation
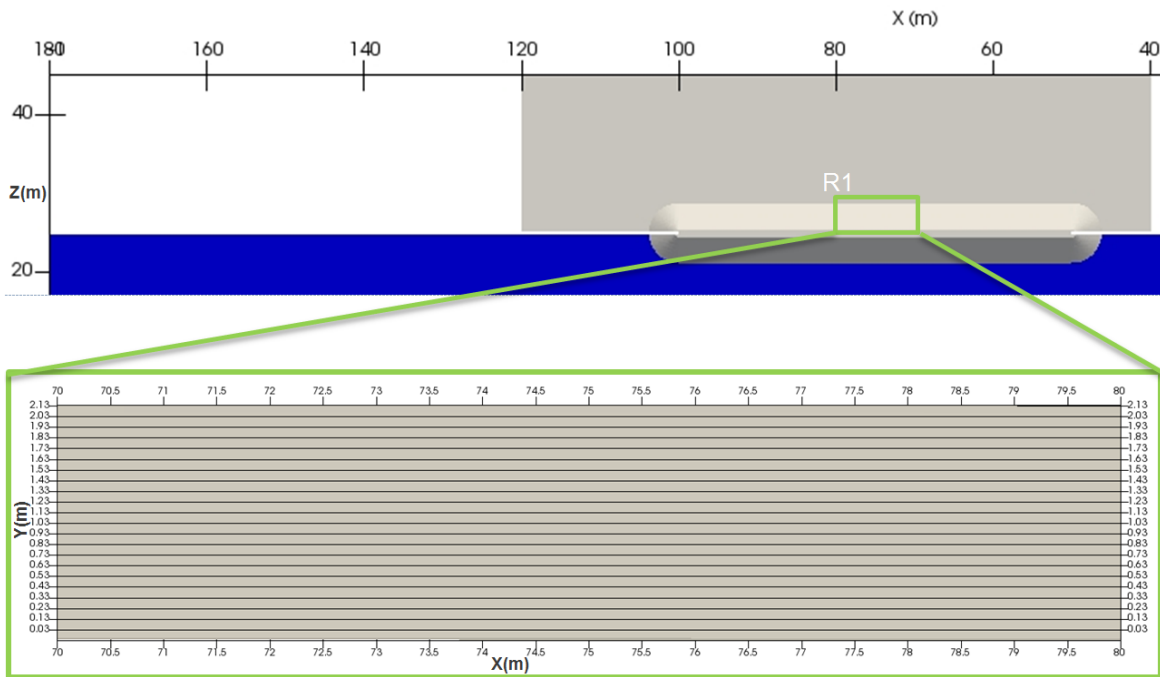
Figure 10.10: Reference segment (R1) of rear side of the lower embankment (Top) and close-up view of the referencing layers used for the analyses

Here is a list of all figures for each test case:

Test case	Figure number	Results illustrated
Case 1	4.3 4.7 4.11 4.15 4.16	Velocity field Velocity amplification factor Velocity field and water surface at longitudinal cross sections (Z=±20) Shear stress at reference segment (as illustrated in Figure 10.10) Shear stress normalised patterns at the 4 roundhead (Figure 10.10)
Case 2	4.4 4.8 4.12 4.17 4.18	Velocity field Velocity amplification factor Velocity field and water surface at longitudinal cross sections (Z=±20) Shear stress at reference segment (as illustrated in Figure 10.10)

		Shear stress normalised patterns at the 4 roundhead (Figure 10.10)
Case 3	4.5 4.9 4.13 4.19 4.20	Velocity field Velocity amplification factor Velocity field and water surface at longitudinal cross sections (Z=±20) Shear stress at reference segment (as illustrated in Figure 10.10) Shear stress normalised patterns at the 4 roundhead (Figure 10.10)
Case 4	4.6 4.10 4.14 4.21 4.22	Velocity field Velocity amplification factor Velocity field and water surface at longitudinal cross sections (Z=±20) Shear stress at reference segment (as illustrated in Figure 10.10) Shear stress normalised patterns at the 4 roundhead (Figure 10.10))

Here is a list of all result tables for each test case:

Test case	Table number	Results presented
Case 1	4.1	Value of the averaged shear stress for each layer
Case 2	4.2	Value of the averaged shear stress for each layer
Case 3	4.3	Value of the averaged shear stress for each layer
Case 4	4.4	Value of the averaged shear stress for each layer

10.4.2 Velocities
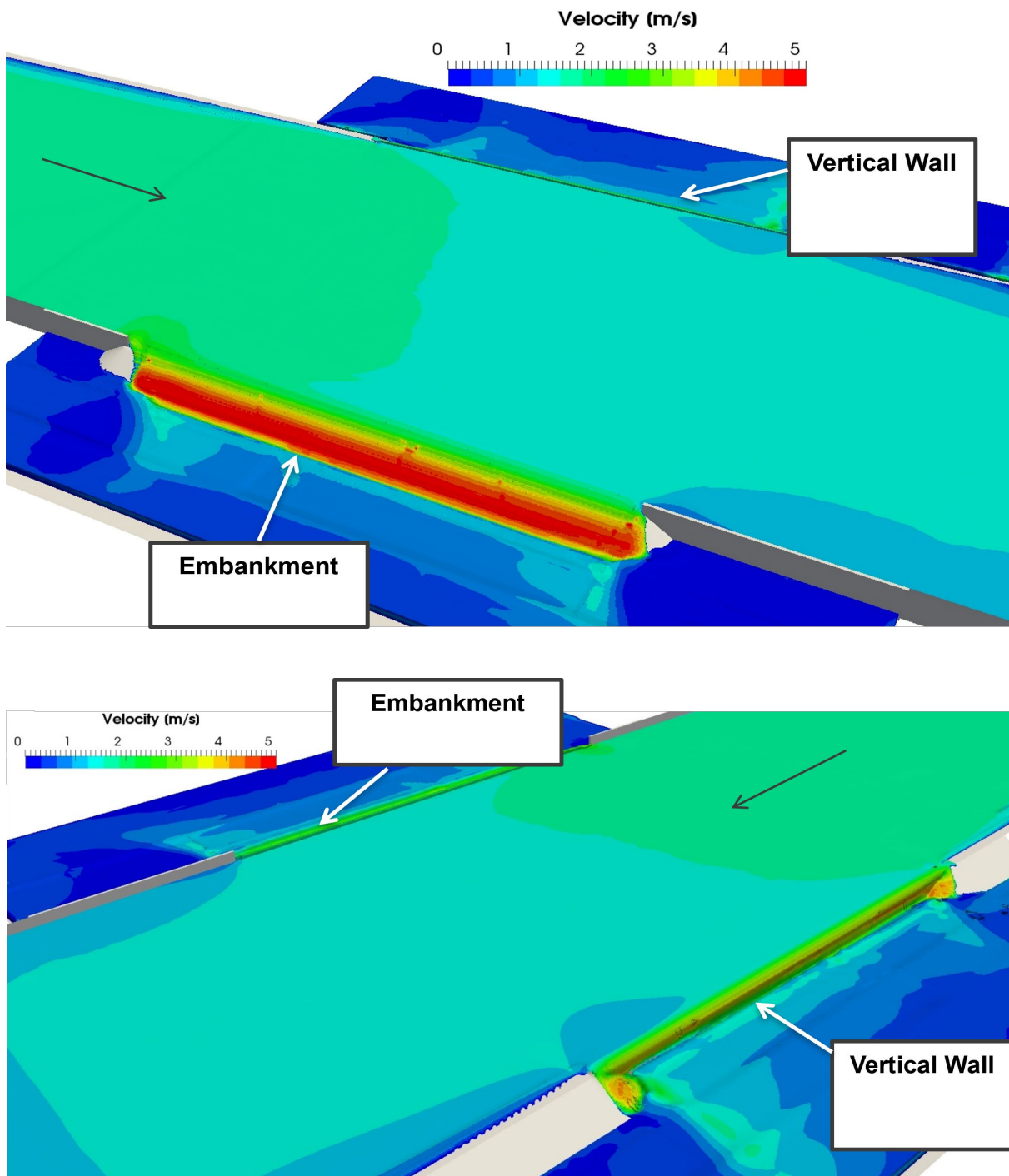
Figure 10.11: Case 01 - 3D views of the time-average flow velocity field. Embankment side view (top) and vertical wall side view (bottom) – Arrow indicates the flow direction
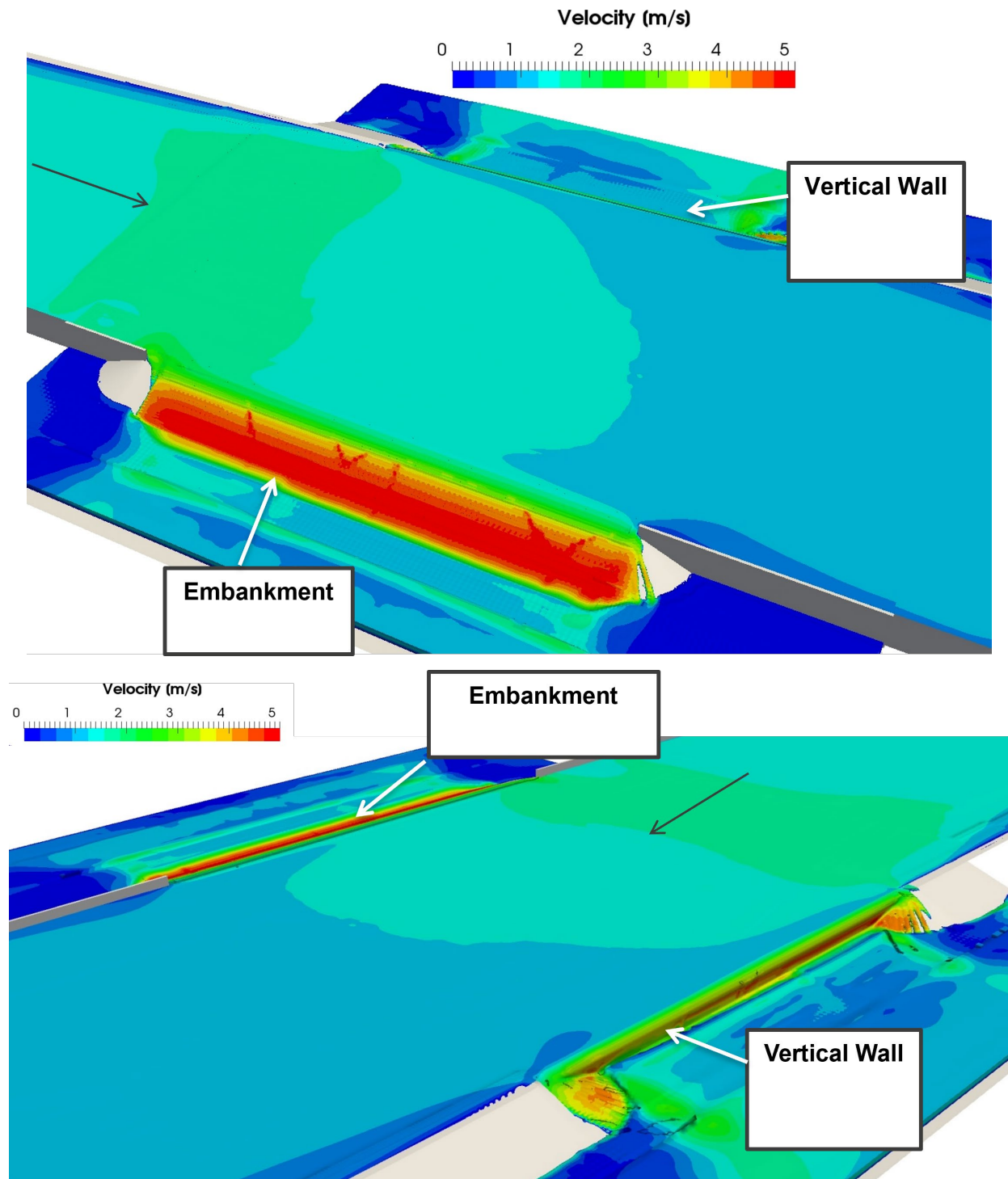
Figure 10.12: Case 02 - 3D views of the time-average flow velocity field. Embankment side view (top) and vertical wall side view (bottom) – Arrow indicates the flow direction
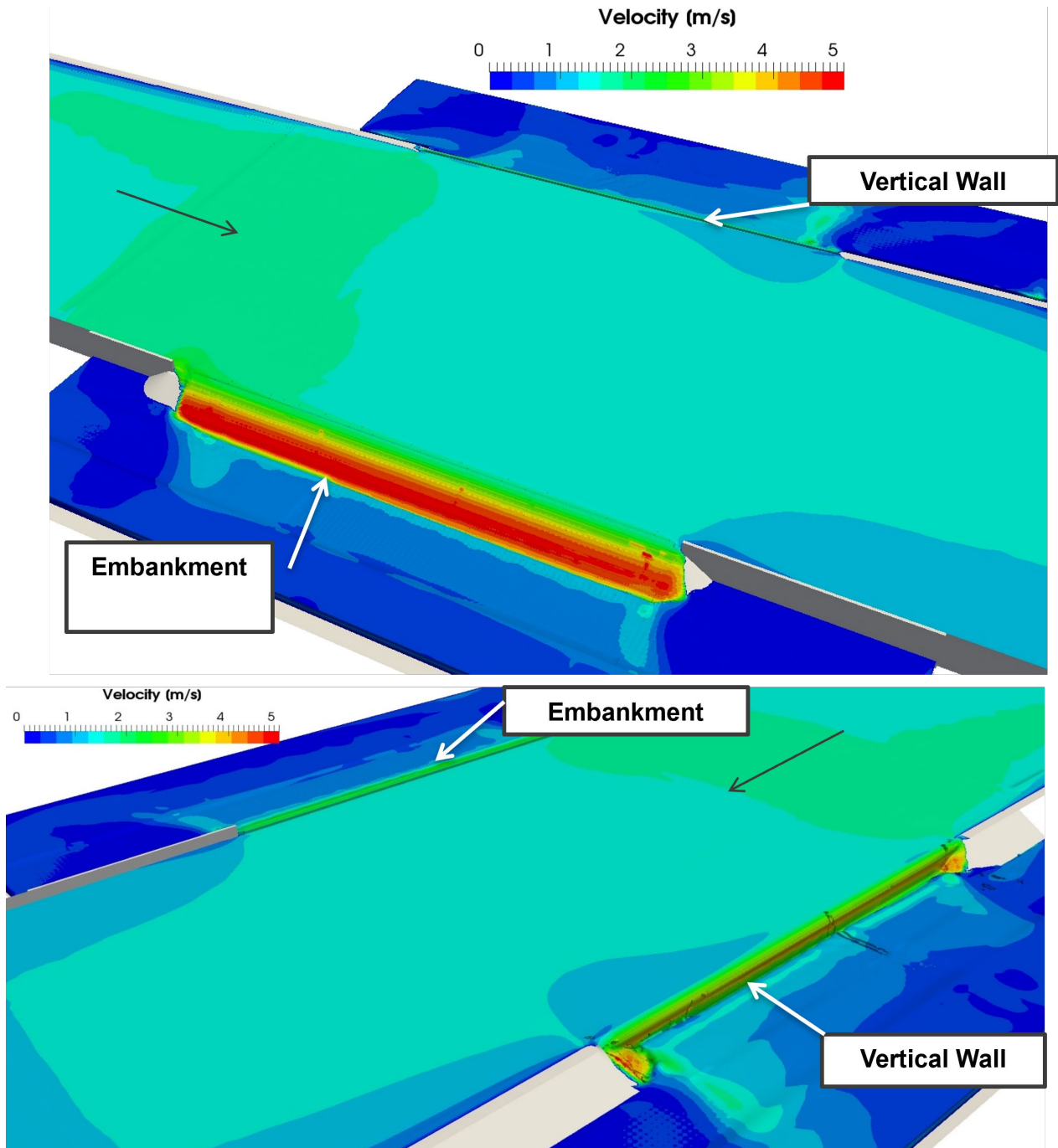
Figure 10.13: Case 03 - 3D views of the time-average flow velocity field. Embankment side view (top) and vertical wall side view (bottom) – Arrow indicates the flow direction
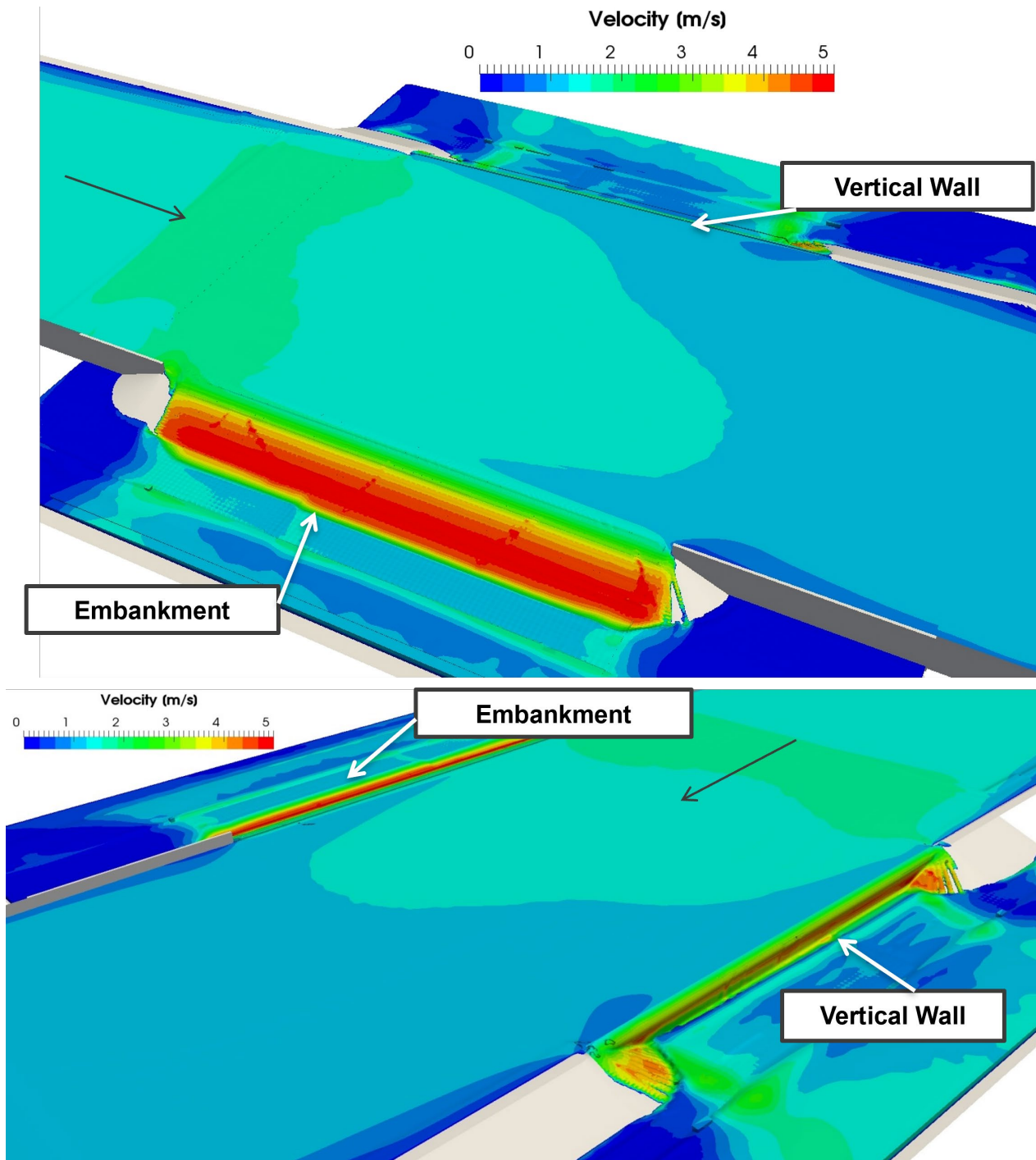
Figure 10.14: Case 04 - 3D views of the time-average flow velocity field. Embankment side view (top) and vertical wall side view (bottom) – Arrow indicates the flow direction
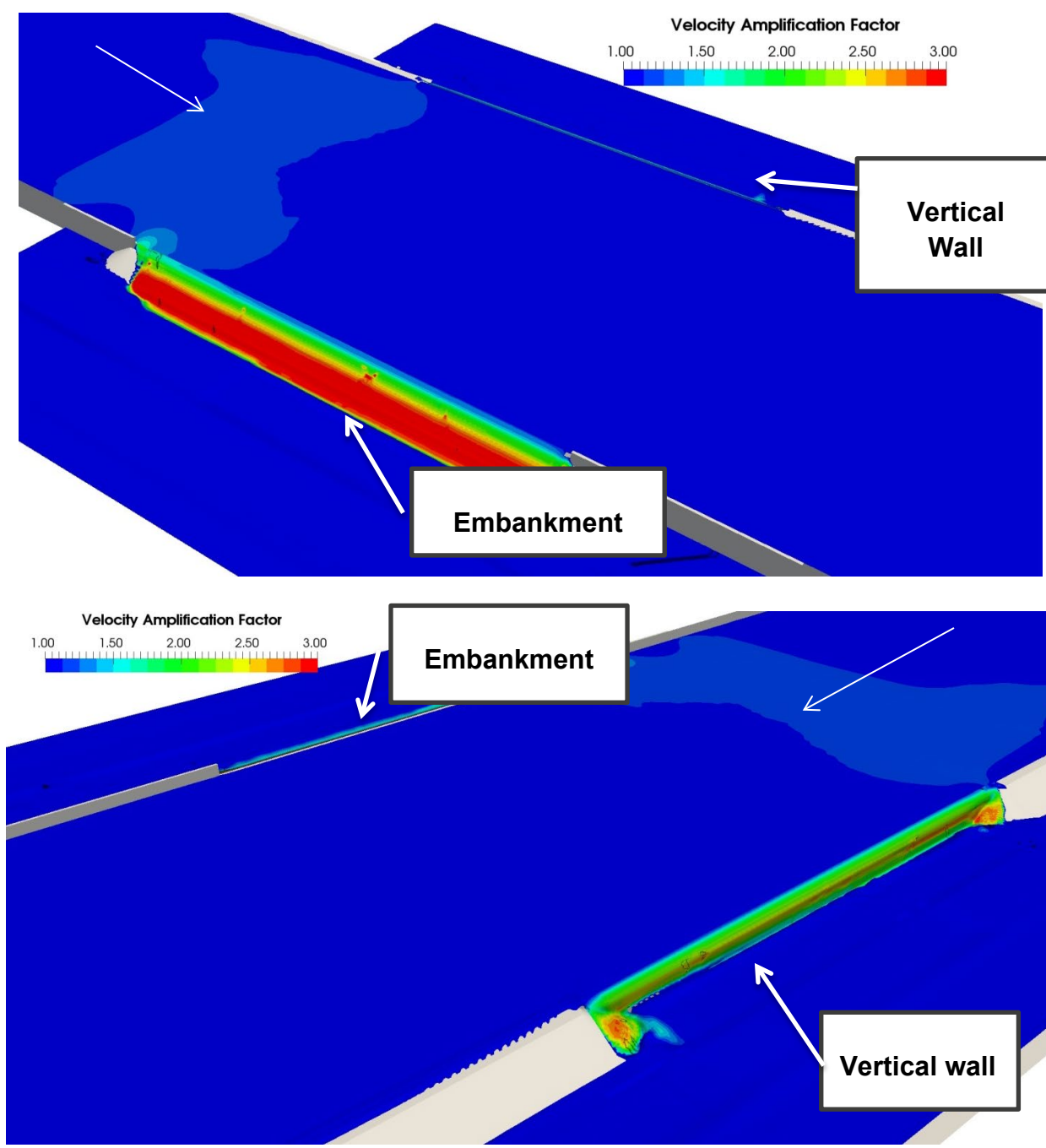
Figure 10.15: Case 01 - Velocity amplification factor at the free-surface. Embankment side view (top) and vertical wall side view (bottom). The factor is express as the ratio between the local time-averaged velocity and a characteristic velocity value of 1.5 m/s. Arrow indicates the flow direction
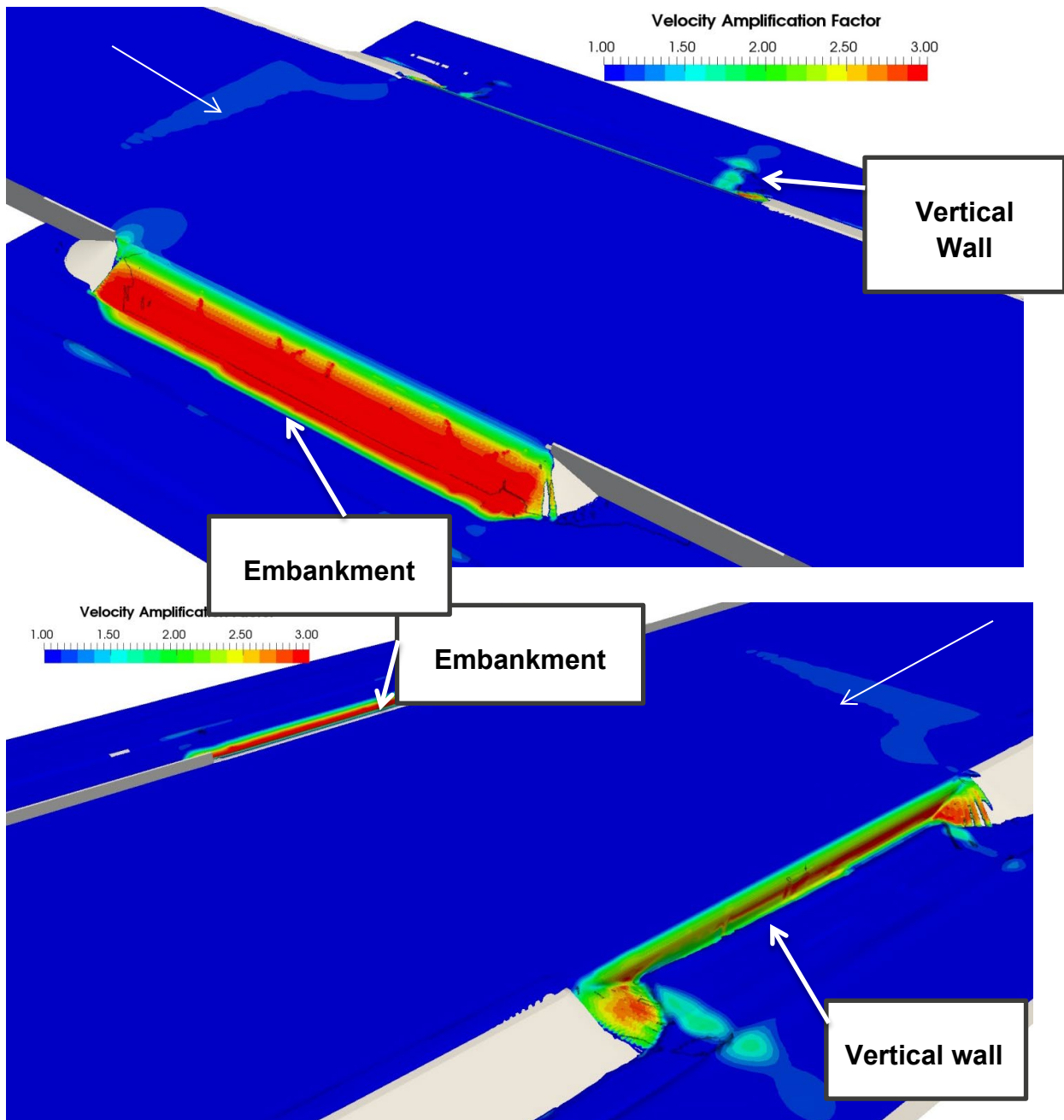
Figure 10.16: Case 02 - Velocity amplification factor at the free-surface. Embankment side view (top) and vertical wall side view (bottom). The factor is express as the ratio between the local time-averaged velocity and a characteristic velocity value of 1.5m/s. Arrow indicates the flow direction
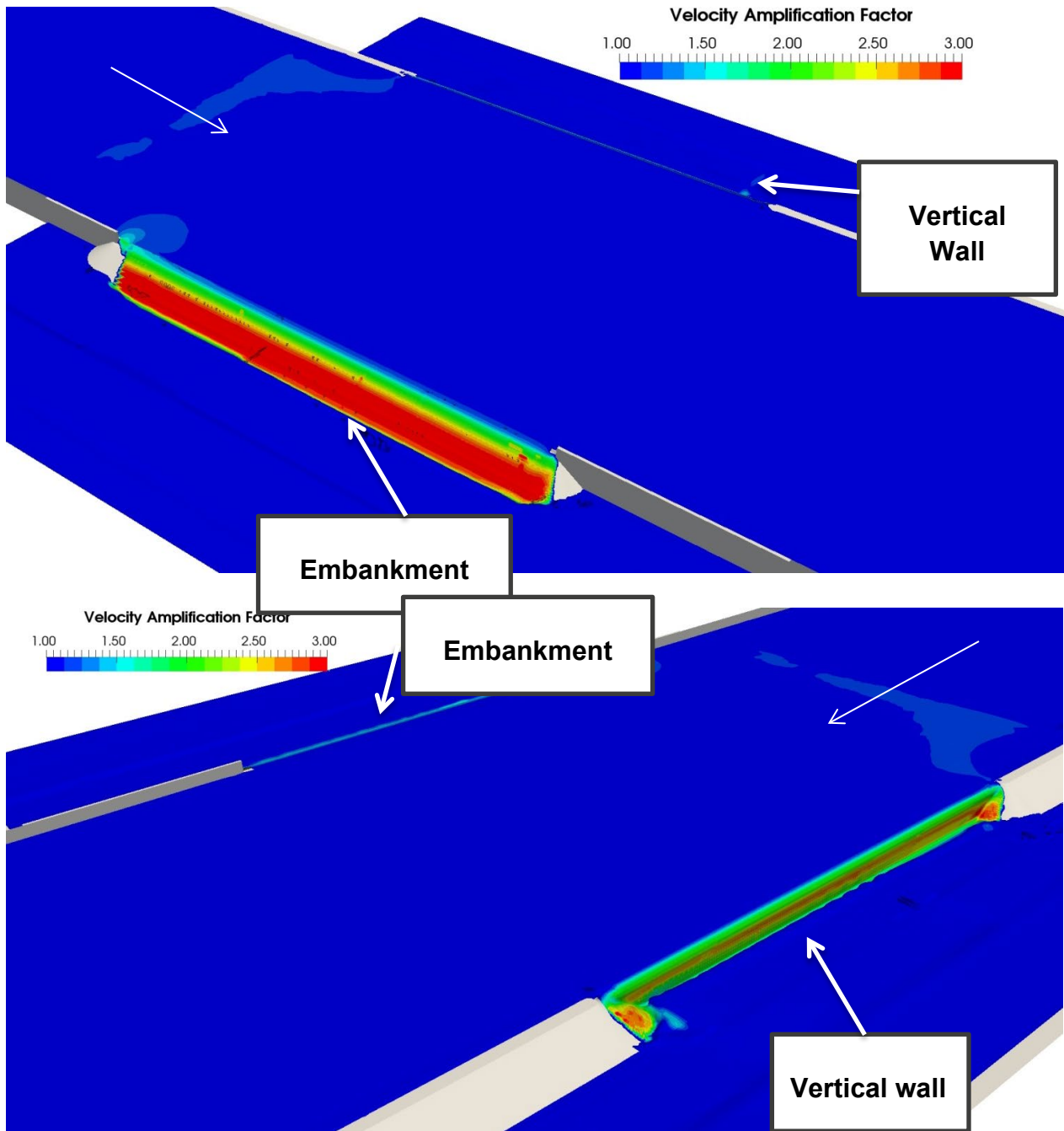
Figure 10.17: Case 03 - Velocity amplification factor at the free-surface. Embankment side view (top) and vertical wall side view (bottom). The factor is express as the ratio between the local time-averaged velocity and a characteristic velocity value of 1.5m/s. Arrow indicates the flow direction
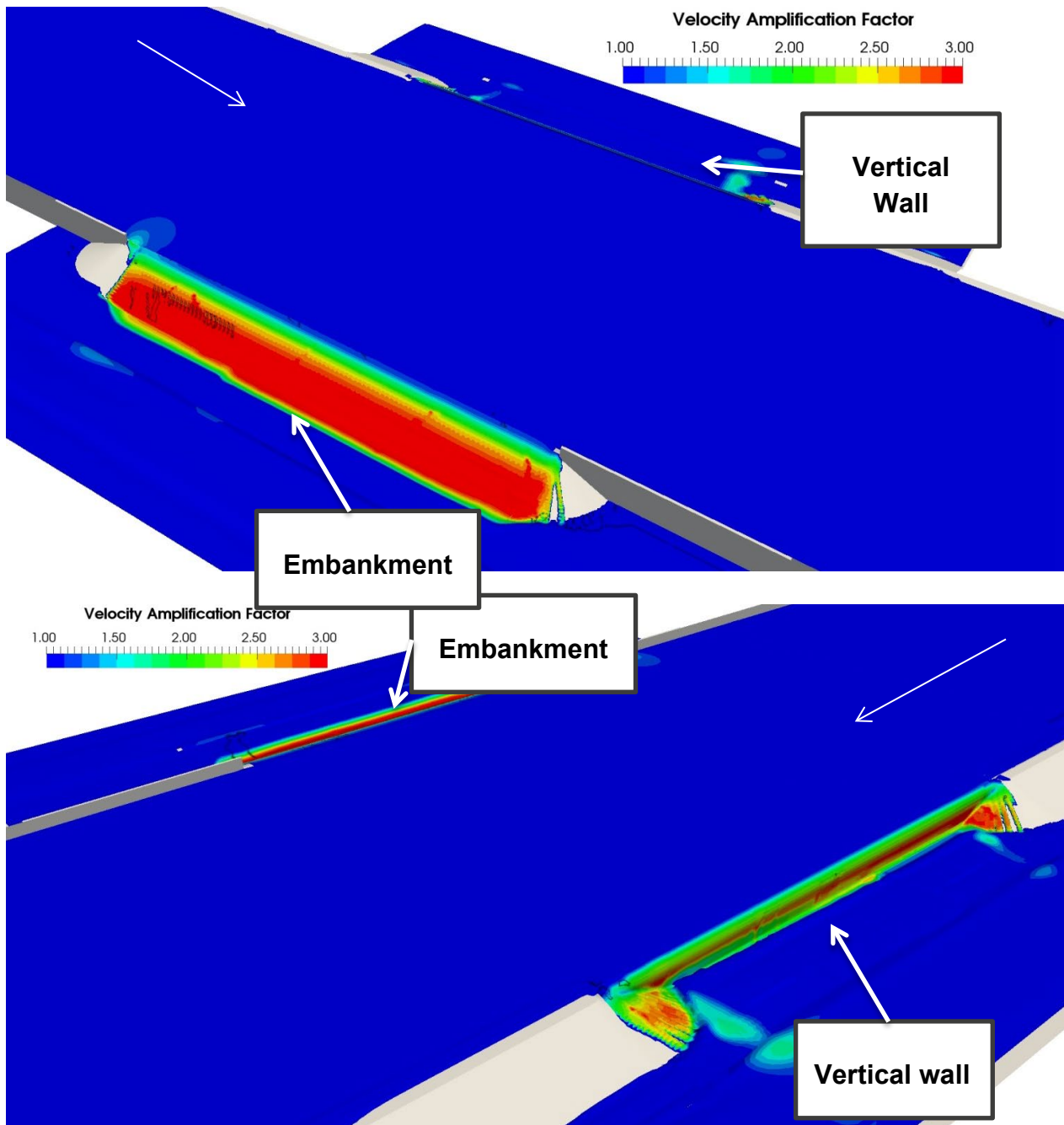
Figure 10.18: Case 04 - Velocity amplification factor at the free-surface. Embankment side view (top) and vertical wall side view (bottom). The factor is express as the ratio between the local time-averaged velocity and a characteristic velocity value of 1.5m/s. Arrow indicates the flow direction
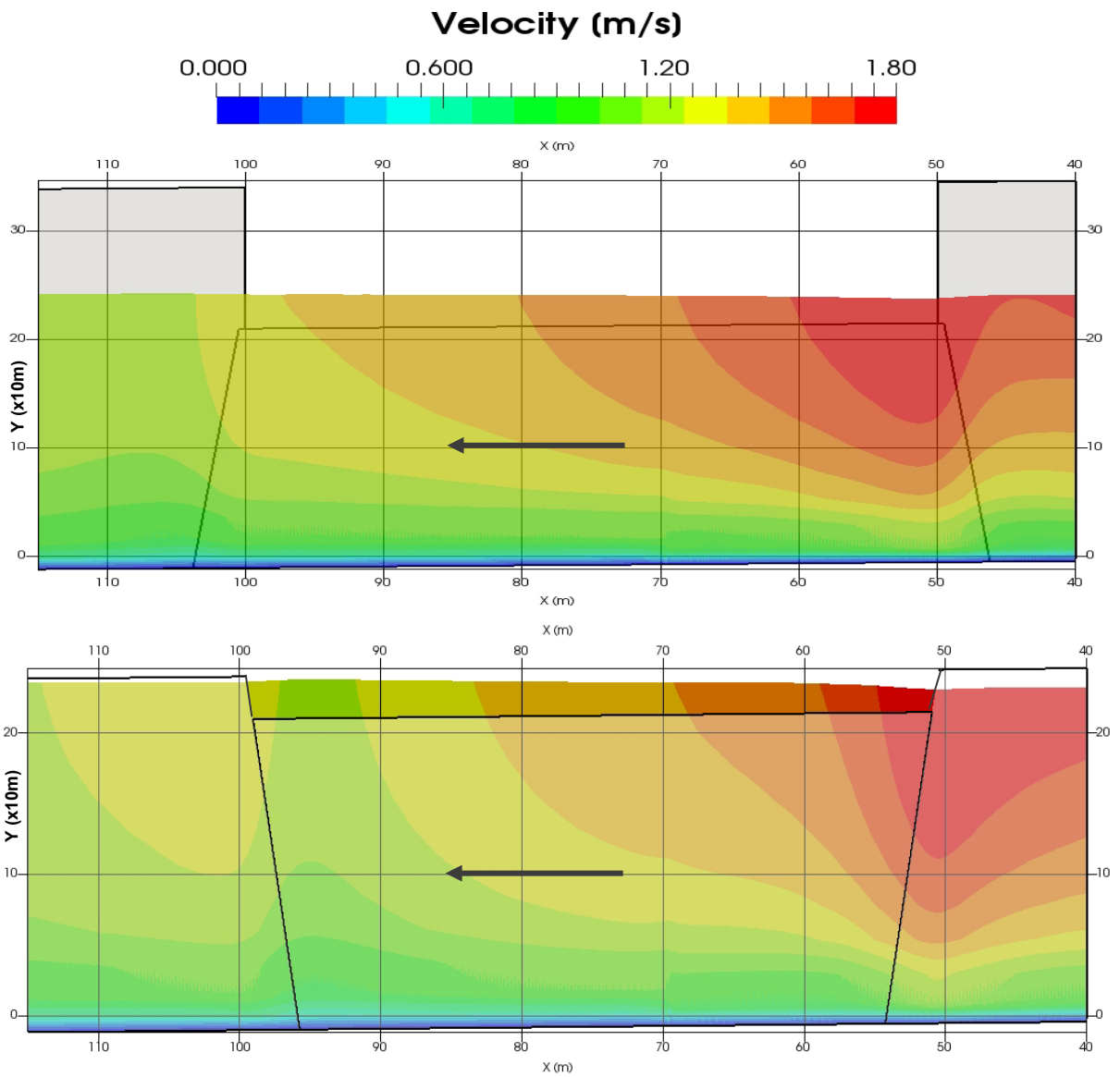
Figure 10.19: Case 01 - Longitudinal cross sections (S1, top and S2, bottom) showing the time-average velocity field. The vertical axis is distorted x 10 times. Arrow indicates the flow direction
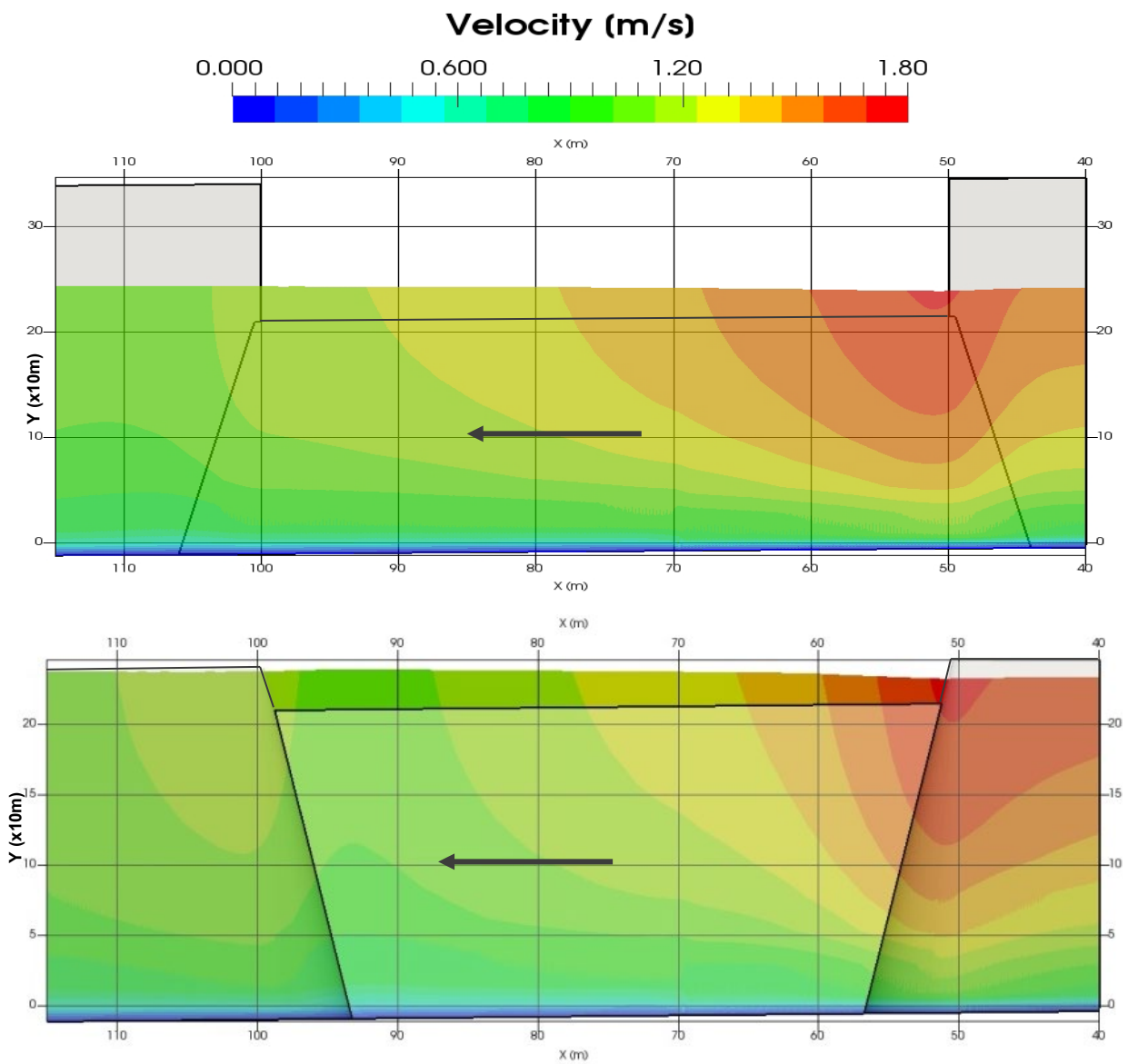
Figure 10.20: Case 02 - Longitudinal cross sections (S1, top and S2, bottom) showing the time-average velocity field. The vertical axis is distorted x 10 times. Arrow indicates the flow direction
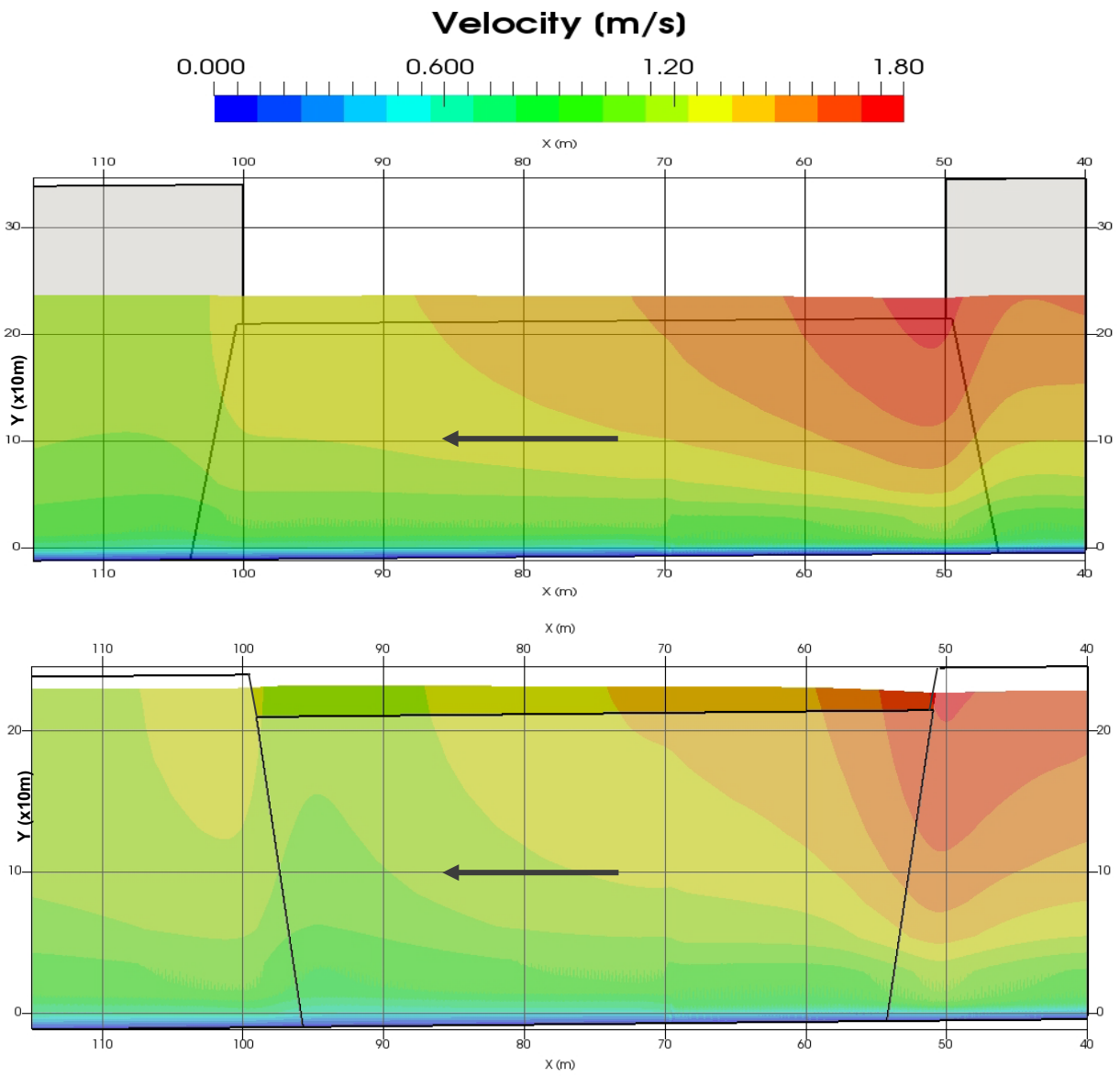
Figure 10.21: Case 03 - Longitudinal cross sections (S1, top and S2, bottom) showing the time-average velocity field. The vertical axis is distorted x 10 times. Arrow indicates the flow direction
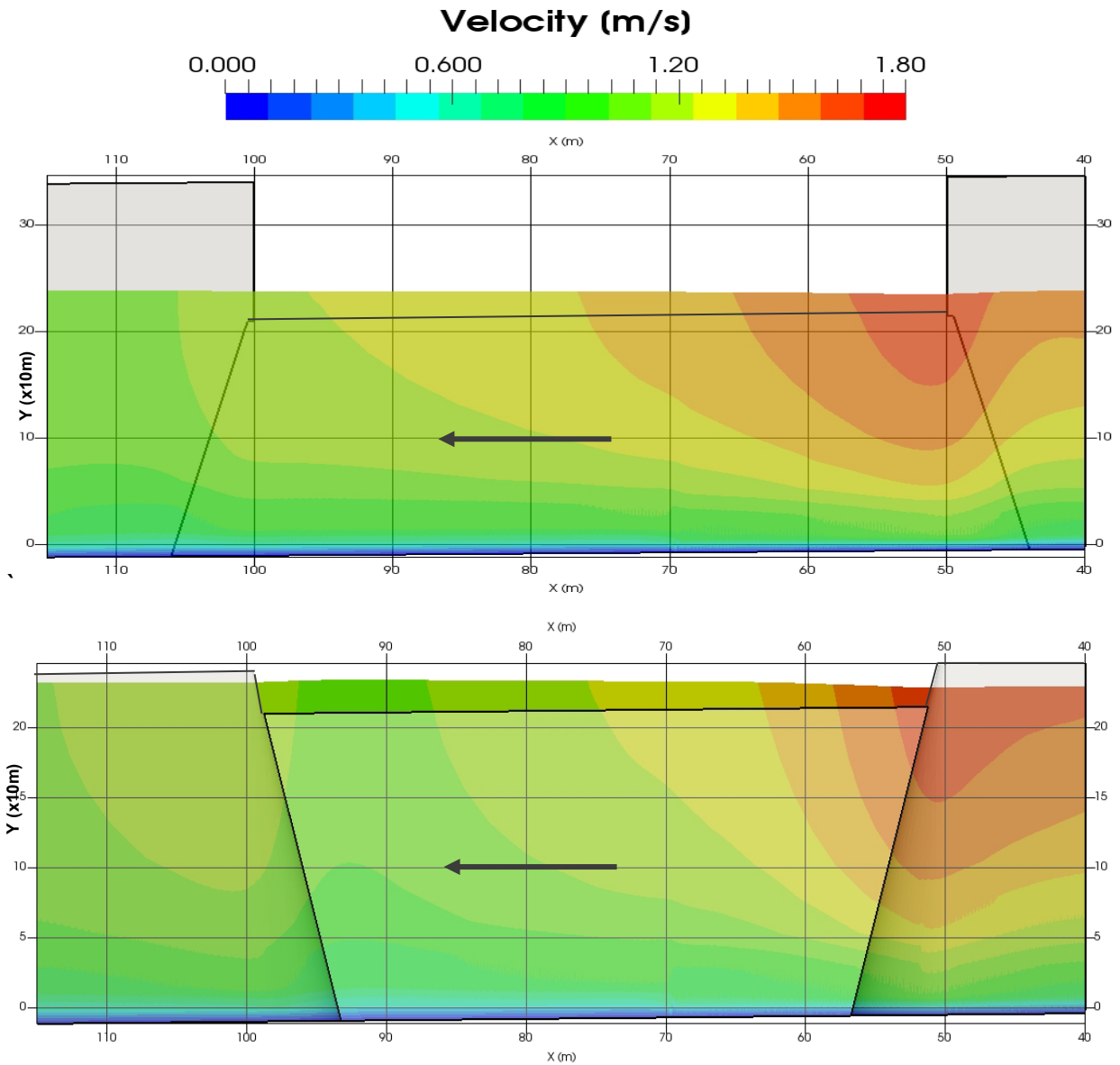
Figure 10.22: Case 04 - Longitudinal cross sections (S1, top and S2, bottom) showing the time-average velocity field. The vertical axis is distorted x 10 times. Arrow indicates the flow direction

10.4.3 Shear stresses – Calculation method 1
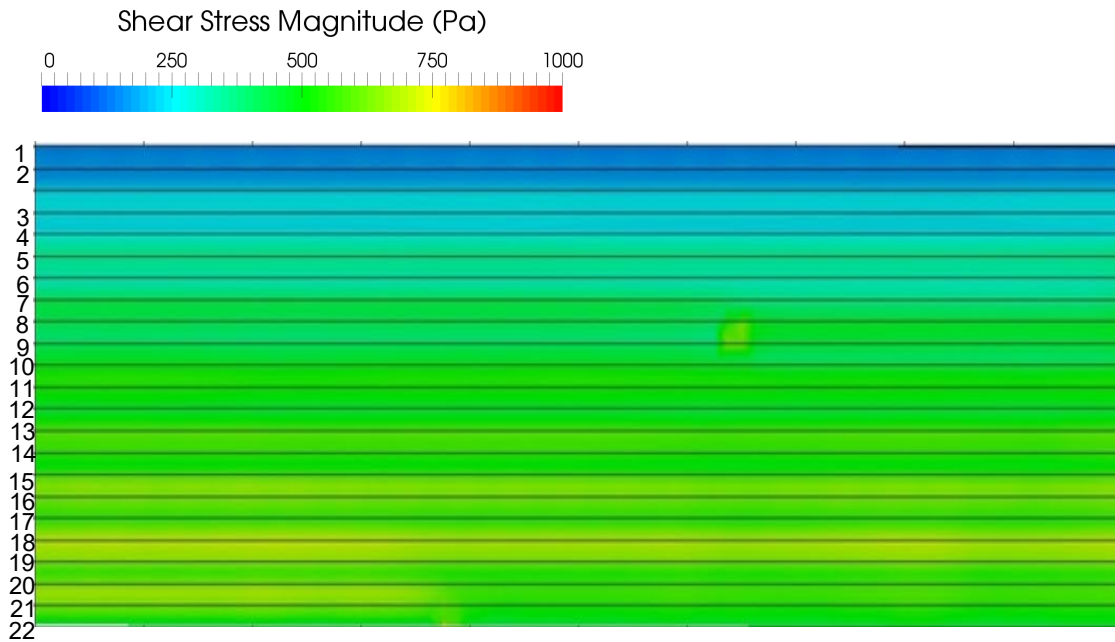
Figure 10.23: Case 01 - Typical shear stress values on the rear side of the lower embankment (R1 in Figure 10.10)

Table 10.2: Value of the averaged shear stress for each layer

Layer No.	Averaged Tau[Pa]
1	123.8
2	199.7
3	255.7
4	258.7
5	316.2
6	341.7
7	341.2
8	415.1
9	424.7
10	431.4
11	500.3
12	493.2
13	490.5
14	563.5
15	517.2
16	596.4

17	582.8
18	579.2
19	653.5
20	572.4
21	581.7
22	363.6
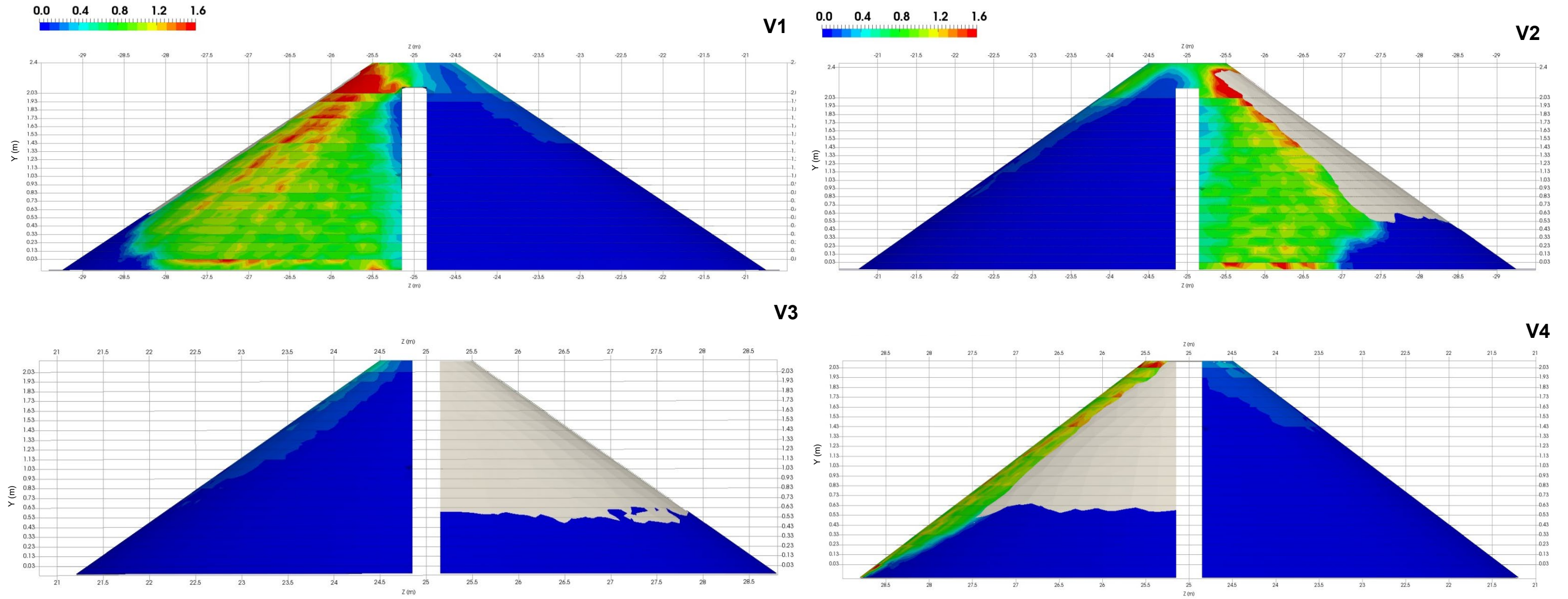
Figure 10.24: Case 01 – Shear stress normalised with respect to the average shear stress at the reference segment presented in Figure 10.23
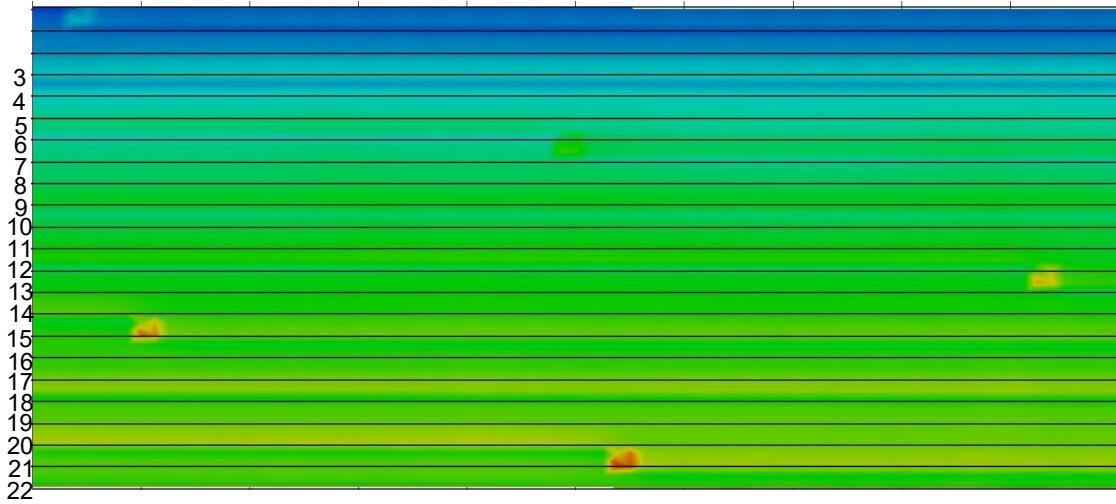
Figure 10.25: Case 02 - Typical shear stress values on the rear side of the lower embankment (R1 in Figure 10.10)

Table 10.3: Value of the averaged shear stress for each layer

Layer No.	Averaged Tau[Pa]
1	120.7
2	182.1
3	239.6
4	253.1
5	299.4
6	342.0
7	366.2
8	376.7
9	438.4
10	423.3
11	460.4
12	499.9
13	478.4
14	511.8

15	525.7
16	532.9
17	567.6
18	607.4
19	568.1
20	625.2
21	611.3
22	500.2
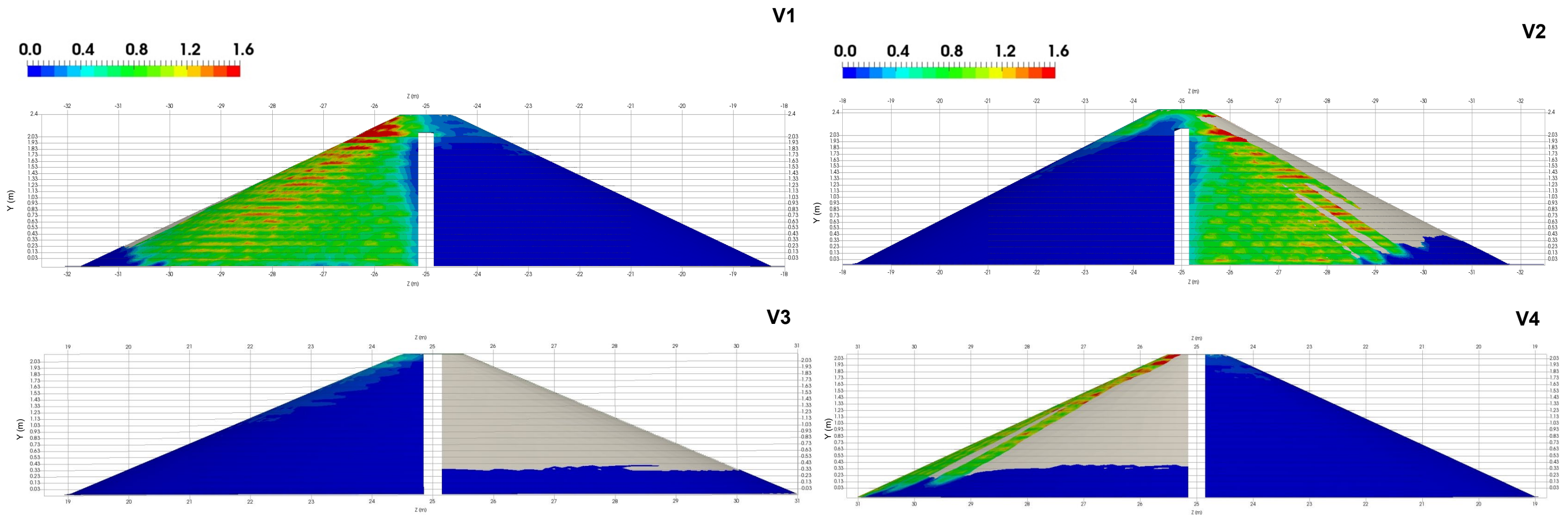
Figure 10.26: Case 02 – Shear stress normalised with respect to the average shear stress at the reference segment presented in Figure 10.10
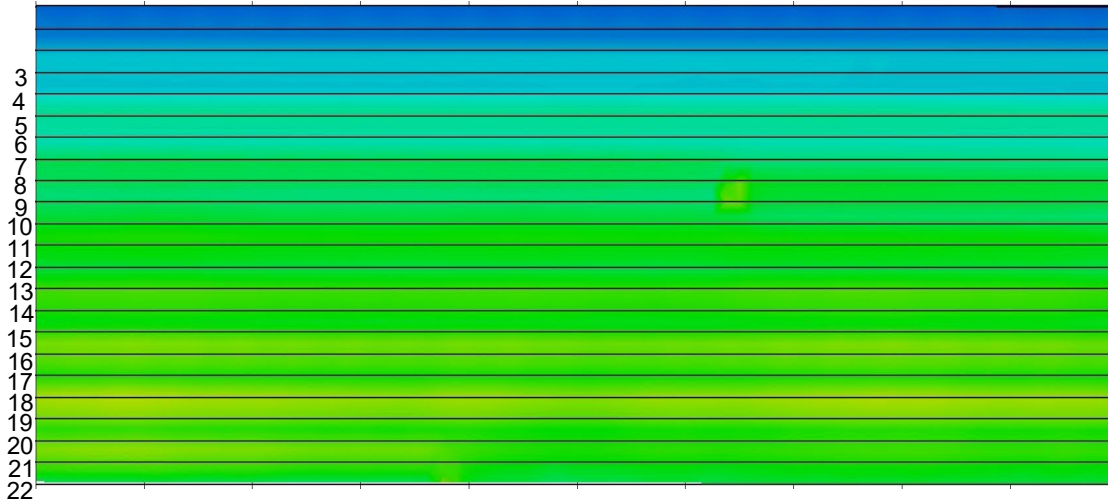
Figure 10.27: Case 03 - Typical shear stress values on the rear side of the lower embankment (R1 in Figure 10.10)

Table 10.4: Value of the averaged shear stress for each layer

Layer No.	Averaged Tau[Pa]
1	109.9
2	185.3
3	242.1
4	247.5
5	306.0
6	332.1
7	333.2
8	406.0
9	415.3
10	421.1
11	488.1
12	481.4
13	479.9
14	552.3

15	507.5
16	585.4
17	572.1
18	572.7
19	638.4
20	556.3
21	560.8
22	543.5
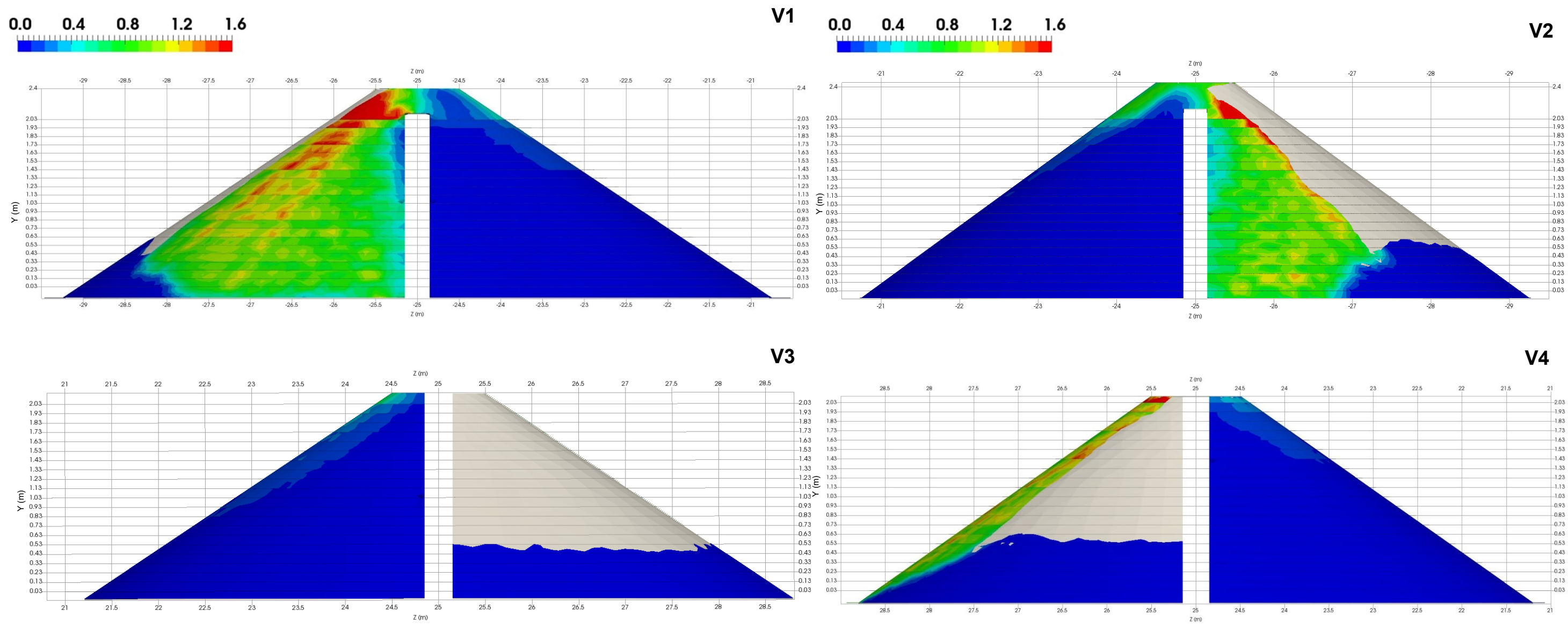
Figure 10.28: Case 03 – Shear stress normalised with respect to the average shear stress at the reference segment presented in Figure 10.27
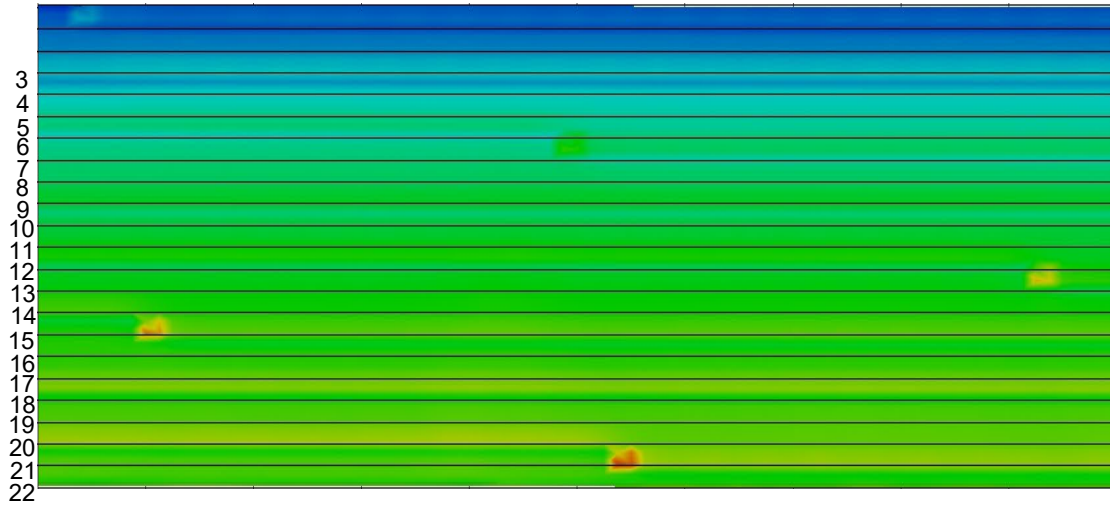
Figure 10.29: Case 04 - Typical shear stress values on the rear side of the lower embankment (R1 in Figure 10.10)

Table 10.5: Value of the averaged shear stress for each layer

Layer No.	Averaged Tau[Pa]
1	108.7
2	171.1
3	229.4
4	241.2
5	291.1
6	332.5
7	356.4
8	367.2
9	427.5
10	413.3
11	450.8
12	490.7
13	471.0
14	504.4

15	554.0
16	524.8
17	520.8
18	514.0
19	509.6
20	498.4
21	485.9
22	485.9
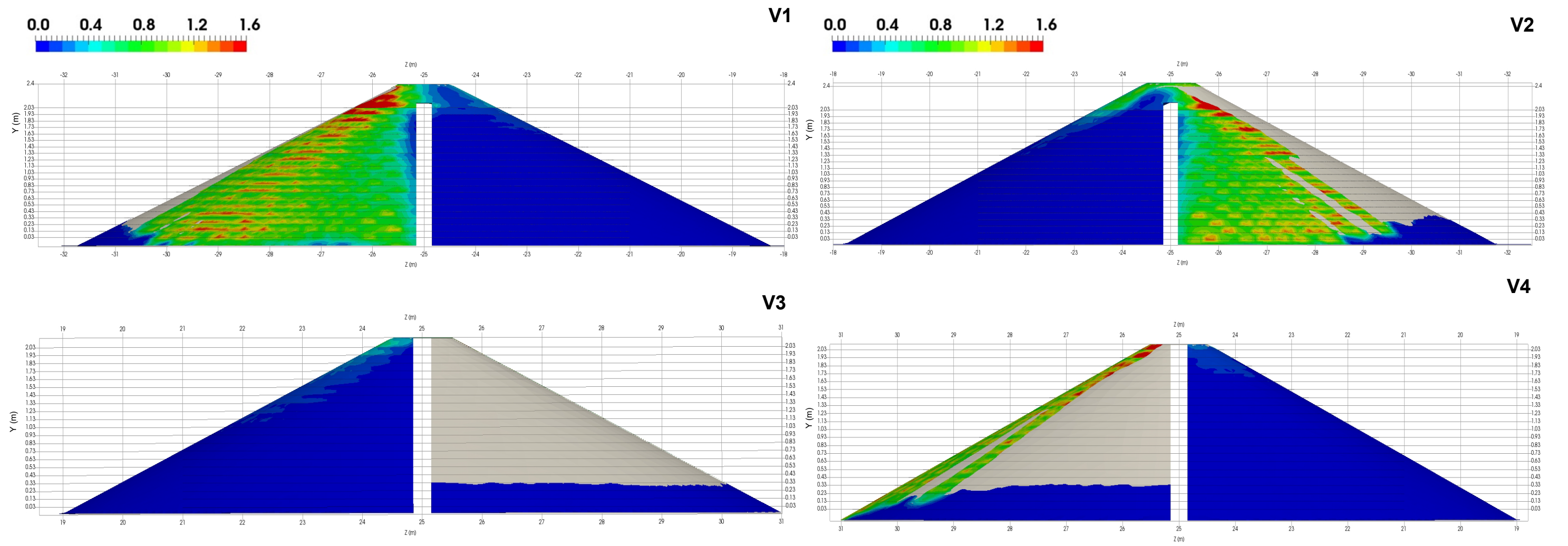
Figure 10.30: Case 04 – Shear stress normalised with respect to the average shear stress at the reference segment presented in Figure 10.29

10.5 Discussion and recommendations

A CFD modelling study was carried out for a typical river section under extreme flood conditions. The geometry of the section considered transitions between 2 different types of flood defences; i) a flood wall 30cm thick and ii) embankments with crown width of 1m and slopes of 1 V: 1.5 H and 1 V:2.5 H. A height difference was assumed between transitions, and the lower section was assumed to be lower than the main river water level, therefore allowing an overflow discharge to develop. The main river flow was assumed to have an average velocity of 1.5m/s and be running under a downstream slope of 0.1%. The geometry was modelled using the open-source CFD tool OpenFOAM®.

Results were presented in terms of velocity amplifications and shear stress amplifications. The amplification of the shear stress at the transitions was calculated in comparison with the level of shear stresses at main trunk of the overflowed structure. Model results suggest that there is an amplification of shear stress of ~1.5 to 2 times in most cases.

The results from the CFD model provide an initial estimate of the overall level of shear stress amplification in these transitions. During interpretations of the results, it should be taken into account that the CFD model is subject to the following limitations, which may affect locally the evolution of velocity and shear:

- turbulence model (k-omega SST) which is based on empirical assumptions
- shear stress calculations subject to wall function theory, which is not generally well posed in flow detachment areas
- effect of aerated flow, especially with respect to bubbles/splashes and small scale air pockets, is subject to uncertainties as mesh refinement is limited to ~10cm due to practical limitations.

Results on shear stresses could be further refined by building on the current study and using a more refined approach. This could include a focus on the local area of transition, using a much more refined mesh (for example, in the order of mm), combined with a more sophisticated (but more expensive) turbulence model, such as a large eddy simulation approach.

References

LEWIN, J., 1981. British rivers. George Allen & Unwin. London.

SAMUELS, P., 1989. Backwater lengths in rivers. Proc. Instn. Engrs. part 2, 87, Dec., 571-582.

WILLIAMSON, P., OGUNYOYE, F., DENNIS, I., DOUGLAS, J., HARDWICK, M., SAYERS, P., FISHER, K., THORNE, C., HOLMES, N., 2015. Channel management handbook. Report SC110002. Published by the Environment Agency.

Acronyms

CFD- computational Fluid Dynamics

LSE – Limit State Equations

IPR – Intellectual property rights

ILH – International Levee Handbook

ICOLD – International Commission on Large Dams

I_{HET} - A measure of how suspectable the soil is to erosion (see table 3)

CIRIA – Construction Industry Research and Information Association

CG – Condition Grade

RAFT+- Risk Assessment Field Tool

CLE – Concentrated Leak Erosion.

NaFRA – National Flood Risk Assessment

APoF – Annual Probability of Failure

LiDAR - Light Detection and Ranging

SST – Shear Stress Transport

Would you like to find out more about us or your environment?

Then call us on

03708 506 506 (Monday to Friday, 8am to 6pm)

Email: enquiries@environment-agency.gov.uk

Or visit our website

www.gov.uk/environment-agency

incident hotline

0800 807060 **(24 hours)**

floodline

0345 988 1188 **(24 hours)**

Find out about call charges (https://www.gov.uk/call-charges)

Environment first

Are you viewing this onscreen? Please consider the environment and only print if absolutely necessary. If you are reading a paper copy, please don't forget to reuse and recycle.